Doctoral Dissertation

CISS (Chirality-Induced-Spin-Selectivity) Effect in Chiral Molecular Superconductor

Department of Structural Molecular Science
School of Physical Sciences
The Graduate University for Advanced Studies, SOKENDAI

Ryota Nakajima

CONTENTS

§1 General Introduction

1-1 Abstract

Superconducting spintronics is a remarkable field of research which combines superconductivity with spintronics to immensely enhance spin-related effects such as spin transport and magnetoresistance[1]. Spin-polarized superconducting current is important for injecting spin into a device and is required to be produced efficiently. However, normal superconducting current doesn't have spin angular momentum because of the singlet nature of Cooper pairs, although triplet state is theoretically predicted. Also, injecting spin from ferromagnetic electrode doesn't significantly affect the entire spin polarization.

Chiral materials can emit a spin-polarized current with a high polarization rate even when it is constituting only light elements. This effect is known as a Chirality-Induced-Spin-Selectivity (CISS) effect[2]. Although various attempts were made to understand CISS effect, no theoretical consensus has been achieved. CISS effect had been observed only for highly insulating materials at its initial stage of research, but now the research has been extended to semiconductors and metals. We have focused our attention on chiral superconductor to further enhance the CISS effect presumably due to its coherent nature that can enhance the spin diffusion length. Macroscopic coherence of the superconducting state may also enable spatial mapping of spin accumulation. In the present study, a spin-polarized transport in a chiral molecular superconductor κ-$(BEDT\text{-}TTF)_2Cu(NCS)_2$ (κ-NCS) is investigated. The strong capability of κ-NCS to orient electrons' spins can be attributed to CISS effect in the superconducting state.

The aim of this dissertation is to develop CISS effect in a superconducting state and to elucidate the relation between chiral superconductor and spin polarization.

1-2 Chirality

When an improper rotation symmetry is breaking, the system becomes chiral and cannot be superimposed onto its mirror image. François Arago discovered that a quartz crystal slice had optical rotation and that colors are produced by interference. Jean-Baptiste Biot observed that quartz plates had right rotational and left rotational crystals by a polarimeter. Louis Pasteur succeeded in optical resolution of tartrate and Jacobus van 't Hoff advocated that carbon atoms adopt a three-dimensional tetrahedral structure to explain the existence of tartrate optical isomers. The word “chirality” was coined by Lord Kelvin.

Chiral molecules are denoted d- and l- based on dextro-rotatory = right-handed $(+)$ and levo-rotatory = left-handed $(-)$, respectively, in the notation of optical isomers. The absolute stereo configurations are denoted (R)- and (S)- derived from Rectus and Sinister, which means upright and left according to the naming priority of the four substituents in the chiral center. The existence of only one isomer in natural chiral molecules is called homochirality, which is one of the unsolved mysteries of life. Catalytic asymmetric synthesis is particularly active in the field of organic chemistry in order to achieve proper drug synthesis and functional liquid crystalline materials.

1-3 Spintronics

Electron magnetic moments originate from electron spins. The manipulation of electron spin degrees of freedom may achieve predominant functions called spintronics further than just electronics. Next-generation devices utilizing spins are expected to contribute to technological innovations such as ultra-large-capacity HDDs, high-sensitivity magnetic sensors, and high-performance non-volatile memories. Triggered by the observation of giant magnetoresistance (GMR) effect[3], the study of spintronics has widely expanded where controlling generation, accumulation, and flow of spins is central issues in a solid state. Charge-to-spin conversion methods have been developed with possible application: spin Hall effect[4] and spin Seebeck effect[5], each corresponding to Hall effect and Seebeck effect. Hall effect shows the production of voltage when an electric current is perpendicular to a magnetic field in a conductor, while Seebeck effect shows that heat is converted into an electric current. Spin Hall effect and Spin Seebeck effect produce spin currents from an electric current and heat, respectively. Inverse effects of them have been reported: inverse Hall effect[6] and spin Peltier effect[7], which can be conducted as a spin detection in a solid state. Whereas the origin of inverse spin Hall effect is initially considered to be spin-dependent Mott scattering due to impurities, it can be explained that carrier's trajectories are deviated due to spin-orbit interaction attributed to asymmetries of the conductor.

The 2D-Hamiltonian with polar point group has the form: $\mathcal{H}_{SO} \propto \boldsymbol{k} \cdot (\boldsymbol{\sigma} \times \boldsymbol{\alpha})$, where k is wave number, σ is the Pauli's matrices, α is electrostatic potential. This 2D-interaction is particularly called Rashba effect[8]. It's also important to discover new routes of generating spin currents. Latest methods report even topological insulators and non-collinear antiferromagnets accomplished them. Spin magnetization induced by an electric current was suggested by Edelstein[9]. Rashba interface builds spin momentum locking accompanying spin-degenerated band structure. Spin splitting is caused by the Rashba effect also. Considering the electron momentum from the wave number space, the energy from Rashba effect is $\boldsymbol{k} \cdot (\boldsymbol{\sigma} \times \boldsymbol{\alpha})$ and the kinetic energy is $\frac{\hbar^2 \boldsymbol{k}^2}{2m}$. This total energy can be described as the following equation:

$$E = \frac{\hbar^2 \boldsymbol{k}^2}{2m} + \boldsymbol{k} \cdot (\boldsymbol{\sigma} \times \boldsymbol{\alpha}) = \frac{\hbar^2}{2m}\left\{\boldsymbol{k}^2 + \frac{2m}{\hbar^2}\boldsymbol{k} \cdot (\boldsymbol{\sigma} \times \boldsymbol{\alpha})\right\} = \frac{\hbar^2}{2m}\left\{\boldsymbol{k} + \frac{2m}{\hbar^2}\frac{(\boldsymbol{\sigma}\times\boldsymbol{\alpha})}{2}\right\}^2 -$$

$$\frac{\hbar^2}{2m}\left\{\frac{2m}{\hbar^2}\frac{(\boldsymbol{\sigma}\times\boldsymbol{\alpha})}{2}\right\}^2.$$

From this equation, the energy band will be split into s positive and s negative branches. Thus, spin split occurs following this dispersion. With the application of an electric current to $-x$ direction, Fermi surface shifts to $+x$ direction, which generates bulk magnetization. The system whose parity is broken produces spin polarization by applying an electric current because the distribution of electrons is shifted (Fig. 1-3-1). This phenomenon is particularly called Rashba-Edelstein effect.

Chiral-Edelstein effect expresses $\boldsymbol{k\sigma\alpha}$ as the energy in a chiral system. In this case, spin is perpendicular to the Fermi surface.

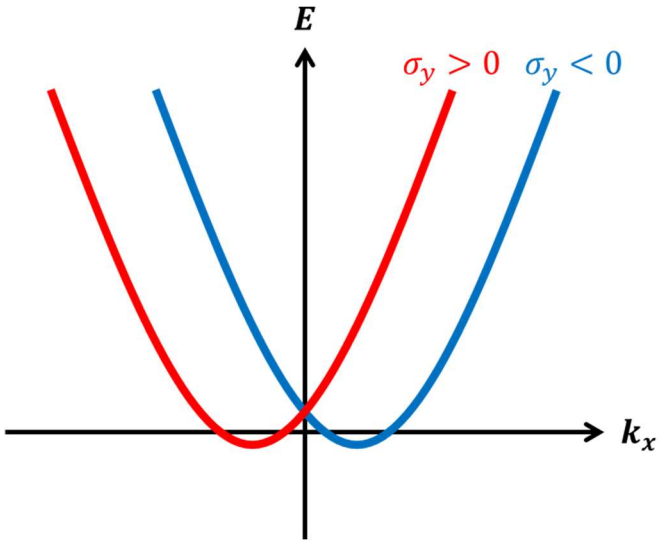

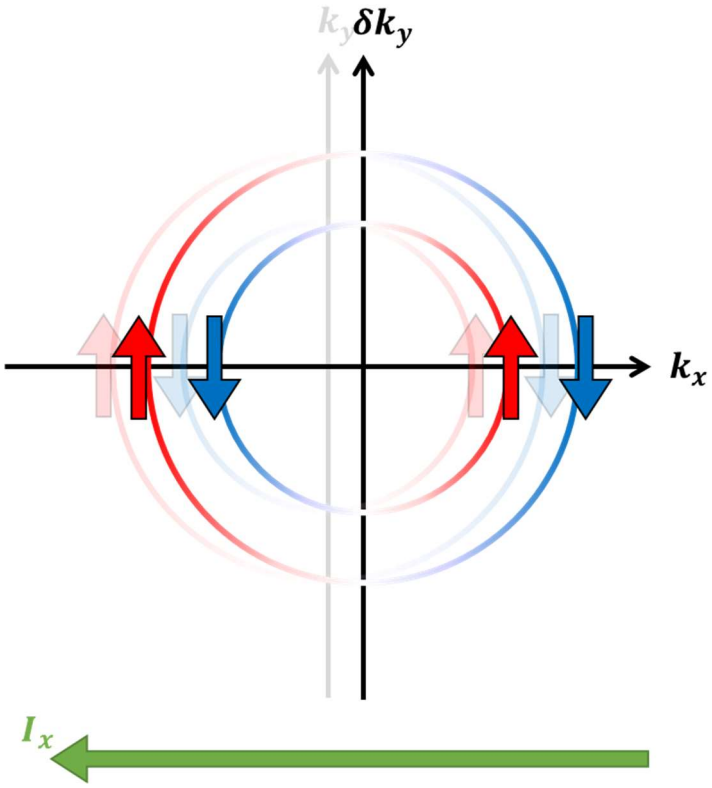

Fig. 1-3-1 Spin splitting electron energy in wave number space. The energy differs depending on the spin orientation in a system without parity symmetry.

2D Edelstein effect mechanism. The current causes the electron density to shift, producing magnetization in Rashba-Edelstein effect.

1-4 Triplet Superconductivity

In many superconductors, the formation of Cooper pairs is isotropic, which is expressed as a s-wave superconductor. In contrast, there are p-, d- and f-wave superconductors where the direction of Cooper pair formation is anisotropic. These are classified according to the symmetry of the Cooper pair order parameter, in which s- and d-waves are spin singlet while p- and f-waves are spin triplet. κ-NCS is d-wave superconductor of which Cooper pair is singlet[10]. In a theoretical investigation by Edelstein, however, it is suggested that p-wave order parameter will emerge in spin-singlet one when a supercurrent is applied in superconductors with noncentrosymmetric lattice[11]. The details of this spin-active superconductivity will be described in the next section.

Spintronics studies have recently covered superconductivity. It seems that a spin polarized superconductor doesn't produce Joule heating in spin transport. Whereas singlet pairing correlation within a Cooper pair is strong, triplet pairing correlations can be found at the magnetized interface between a superconductor and a ferromagnet due to spin-dependent scattering[1]. Triplet supercurrent can be understood by spin-mixing and spin-rotation. Spin-dependent scattering shifts Cooper pair's phase due to Gauge symmetry breaking, occurring on the magnetized interface with the Zeeman field. The triplet Cooper pair can be formed by rotating the quantization axis for one of the paired spins of singlet Cooper pair (Fig. 1-4-1). The lifetime of triplet Cooper pair at the interface is very short in this case even if a spin-polarized current is directly applied to the superconductor. In this regard, generating stable spin-triplet state in bulk superconductor is more promising for future superconducting spintronics devices.

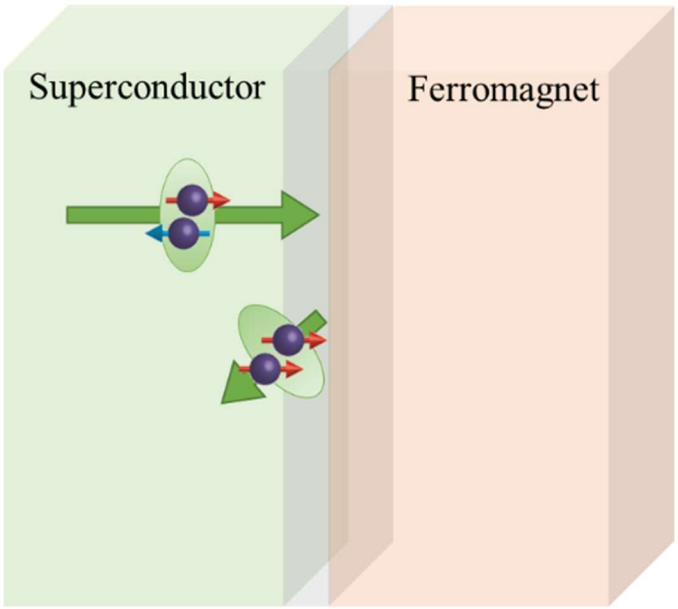

Fig. 1-4-1 Example of a triplet superconductivity generation mechanism. A triplet superconducting current is generated with Gauge symmetry breaking when the superconducting current is scattered at the interface with the ferromagnet.

1-5 Magnetoelectric Effect in Gyrotropic Superconductor

Spin polarization is theoretically predicted to be generated by electric current in a gyrotropic superconductor by Edelstein effect[11]. This is given by $\delta n = \boldsymbol{T}\tilde{\boldsymbol{J}}_{\boldsymbol{e}}$ —— (1), where δn denotes spin polarization density, $\boldsymbol{T}$ denotes a component of the magnetoresistance tensor, and $\tilde{\boldsymbol{J}}_{\boldsymbol{e}}$ denotes a supercurrent density. The magnetoresistance tensor for noncentrosymmetric superconductors is characterized in several point groups[12] (Fig. 1-5-1).

$$C_1: \begin{pmatrix} T_{xx} & T_{xy} & T_{xz} \\ T_{yx} & T_{yy} & T_{yz} \\ T_{zx} & T_{zy} & T_{zz} \end{pmatrix} \quad C_2: \begin{pmatrix} T_{xx} & 0 & T_{xz} \\ 0 & T_{yy} & 0 \\ T_{zx} & 0 & T_{zz} \end{pmatrix} \quad C_3: \begin{pmatrix} T_{\parallel} & 0 & -T^- \\ 0 & T_{yy} & 0 \\ -T^- & 0 & T_{\parallel} \end{pmatrix}$$

$$C_4: \begin{pmatrix} T_{\parallel} & 0 & -T^- \\ 0 & T_{yy} & 0 \\ -T^- & 0 & T_{\parallel} \end{pmatrix} \quad C_{1v}: \begin{pmatrix} 0 & 0 & T_{xz} \\ 0 & 0 & T_{yz} \\ T_{zx} & T_{zy} & 0 \end{pmatrix} \quad C_{2v}: \begin{pmatrix} 0 & 0 & T_{xz} \\ 0 & 0 & 0 \\ T_{zx} & 0 & 0 \end{pmatrix}$$

$$C_{3v}: \begin{pmatrix} 0 & 0 & -T^- \\ 0 & 0 & 0 \\ T^- & 0 & 0 \end{pmatrix} \quad C_{4v}: \begin{pmatrix} 0 & 0 & -T^- \\ 0 & 0 & 0 \\ T^- & 0 & 0 \end{pmatrix} \quad D_2: \begin{pmatrix} T_{xx} & 0 & 0 \\ 0 & T_{yy} & 0 \\ 0 & 0 & T_{zz} \end{pmatrix}$$

$$D_3: \begin{pmatrix} T_{\parallel} & 0 & 0 \\ 0 & T_{yy} & 0 \\ 0 & 0 & T_{\parallel} \end{pmatrix} \quad D_4: \begin{pmatrix} T_{\parallel} & 0 & 0 \\ 0 & T_{yy} & 0 \\ 0 & 0 & T_{\parallel} \end{pmatrix} \quad T: \begin{pmatrix} T_0 & 0 & 0 \\ 0 & T_0 & 0 \\ 0 & 0 & T_0 \end{pmatrix} \quad O: \begin{pmatrix} T_0 & 0 & 0 \\ 0 & T_0 & 0 \\ 0 & 0 & T_0 \end{pmatrix}$$

T_{ij} with $i,j = x,y,z$ are commonly the elements in T. $T_{\parallel}$ denotes the elements T_{xx}, T_{yy} as $T_{\parallel} = T_{xx} = \pm T_{yy}$ and T_0 denotes the diagonal elements in the T and O point group when $T_{xx} = T_{yy} = T_{zz}$. T^- denotes the antisymmetric off-diagonal elements in T, respectively. T_{kj} is a component of the magnetoelectric pseudotensor.

$$T_{kj} = \left\{ \frac{{\Delta_0}^2}{{\boldsymbol{g}_{\boldsymbol{p_F}}}^2} f\left(\frac{|g_{p_F}|}{\pi k_b T_c}\right) \langle J_{kj}(\boldsymbol{p_F}) \rangle + \left[\frac{7{\Delta_0}^2 \zeta(3)}{8\pi^2 {k_b}^2 {T_c}^2} - \right. \right.$$

$$\left. \left. \frac{{\Delta_0}^2}{{\boldsymbol{g}_{\boldsymbol{p_F}}}^2} f\left(\frac{|g_{p_F}|}{\pi k_b T_c}\right) \right] \langle \hat{\boldsymbol{g}}_{\boldsymbol{p_F k}} \hat{\boldsymbol{g}}_{\boldsymbol{p_F i}} J_{ij}(\boldsymbol{p_F}) \rangle \right\} \frac{2\mu_B g}{3\sqrt{3}\xi} N(E_F) \quad \text{—— (3),}$$

where $k = x,y,z$ denotes the component of δn, Δ_0 denotes homogeneous pairing order parameter magnitude, $\boldsymbol{g}_{\boldsymbol{p_F}}$ denotes spin-orbit coupling magnitude, k_b denotes Boltzmann constant, T_c denotes superconducting transition temperature, the rank-two

pseudotensor $J_{ij}(\boldsymbol{p})$ as $J_{ij}(\boldsymbol{p}) = \partial_{p_j} g_i(\boldsymbol{p})$ with $i,j = x,y,z$, and the function $f(\rho)$ as $f(\rho) = Re\sum_{n=0}^{\infty}\left(\frac{1}{2n+1} - \frac{1}{2n+1+i\rho}\right)$. The homogeneous pairing order parameter is a spatially uniform solution (so-called s-wave) satisfying the gap equation, which then corresponds to the superconducting gap. The relation between the superconducting gap and the superconducting transition temperature is well studied in theory and they are proportional: $\frac{\Delta_0}{k_B T_c} \approx 1.76$.

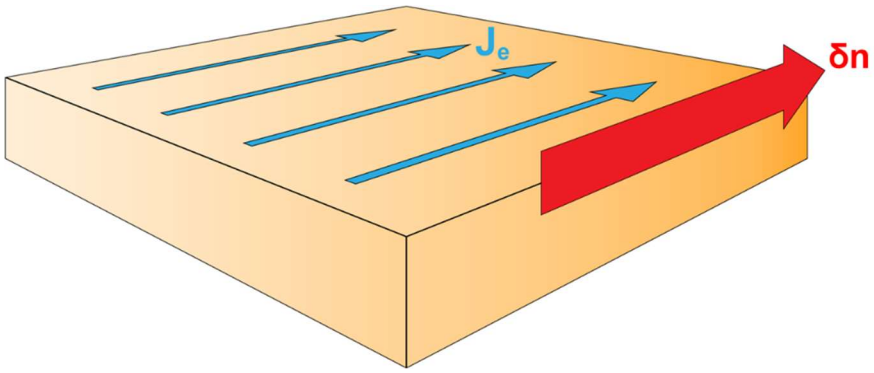

Fig. 1-5-1 A supercurrent-driven magnetization in a superconducting chiral crystal belonging to T and O point groups. Supercurrents arise magnetization which is parallel to the supercurrent direction.

1-6 Chirality-Induced Spin Selectivity (CISS) effect

A spin-polarized electric current can be sometimes produced with a high polarization rate by passing an electric current through a chiral molecule (Fig. 1-6-1). This effect is known as a chirality-induced spin selectivity (CISS) effect[2]. CISS effect at the beginning of its study had been observed only for highly insulating materials. The research has been extended to semiconductors and metals recently. Although various attempts were made to understand CISS effect, no theoretical consensus has been achieved. However, it is possible to quantitatively assume the origin of CISS effect. When an electron passing through the chiral superconductor flows into the electrode, it carries spin polarization generated while an electron experiences electrostatic potential. An electric current generates a magnetic field in a following equation: $\boldsymbol{B} = \boldsymbol{v} \times \boldsymbol{E}_{\boldsymbol{chiral}}$, where $\boldsymbol{B}$ denotes a magnetic flux density, $\boldsymbol{v}$ denotes a moving electron's velocity, and $\boldsymbol{E}_{\boldsymbol{chiral}}$ denotes electrostatic potential of a chiral molecule[14].

CISS effect has been also studied in photoelectron spectroscopy. Double-stranded DNA (dsDNA) is a chiral material. By irradiating linear polarized laser to a polycrystalline (Au)-coated substrate with monolayers of dsDNA, polarized electrons were ejected from the substrate and went through dsDNA[15] (Fig. 1-6-2). The spin polarization rate was up to 60%.

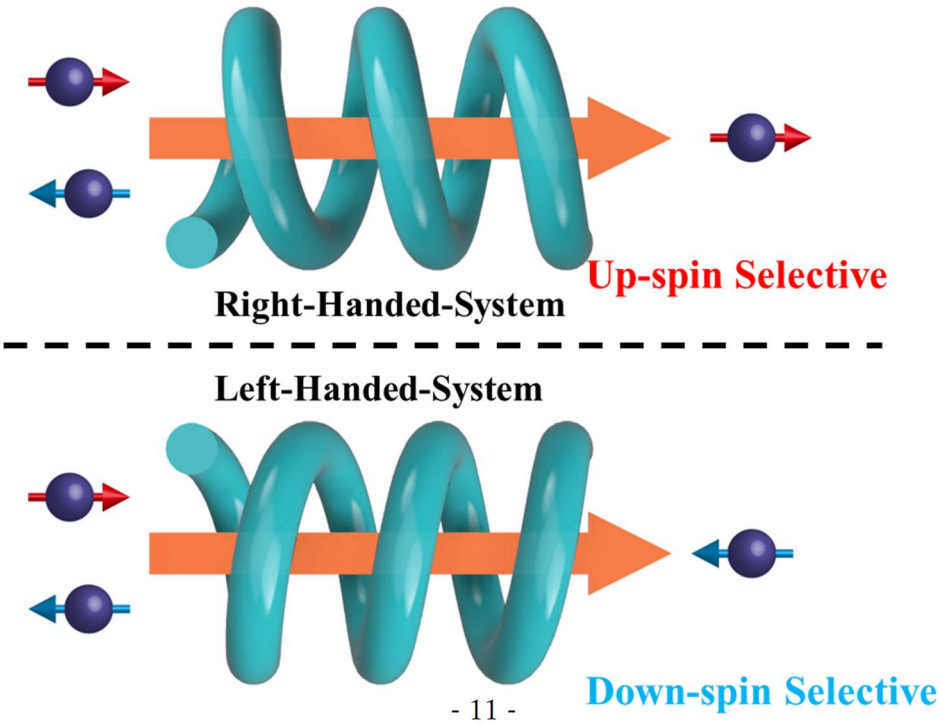

Fig. 1-6-1 Conceptual schematic of CISS effect. Chiral materials emit a spin-polarized electric current of which orientation is determined by the handedness of materials.

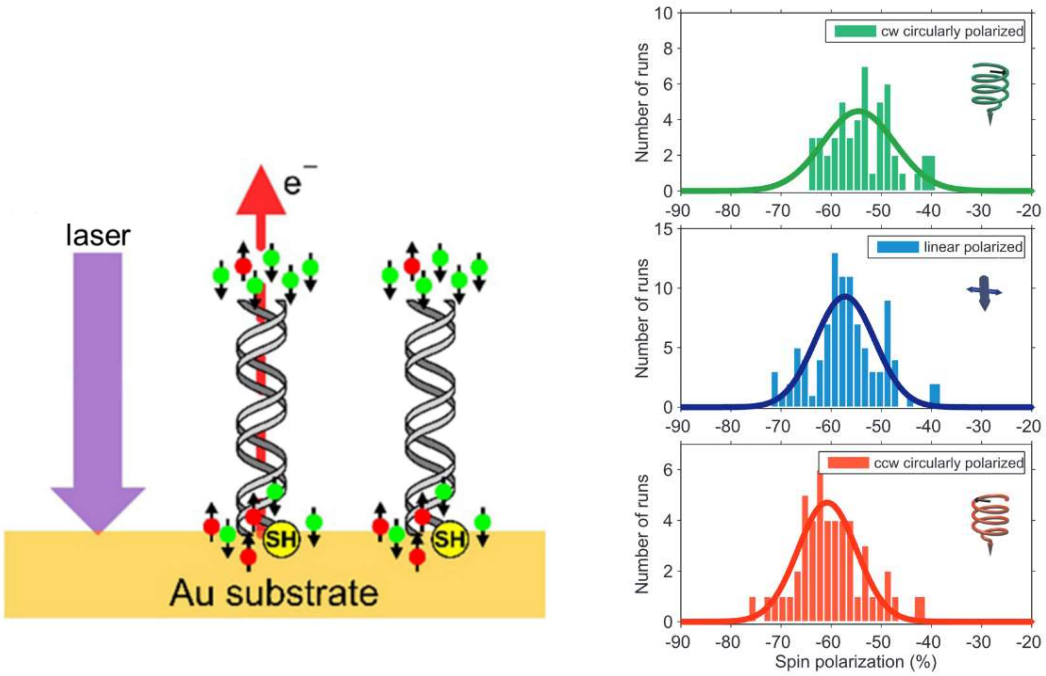

Fig. 1-6-2 Schematics of photoelectron spectroscopy experiment.

The photoelectron polarization as measured for ejecting electrons. High spin polarization rate values of 60% was observed.

1-7 Electrical Magnetochiral Anisotropy

To investigate a chiral-dependent phenomenon, electrical magnetochiral anisotropy (EMChA) must be considered[16]. Normal magnetoresistance (MR) shows that free electrons in a solid can be deviated by a magnetic field. In a chiral material, the amount of change in the magnetoresistance differs depending on the direction of parallel/antiparallel magnetic field to the electric current. The entire electric resistance denotes $R = R_0(1 + \gamma \boldsymbol{B} \cdot \boldsymbol{I})$, where γ is a gyrotropic coefficient, $\boldsymbol{B}$ is a magnetic field, $\boldsymbol{I}$ is an electric current, respectively. Tungsten disulfide is a semiconductor consisted of metal dichalcogenides and forms a chiral nanotube structure. This material exhibits superconductivity under the gating. The magnitude of the resistance value varied depending on the magnetic field direction under the superconducting state[17] (Fig. 1-7-1).

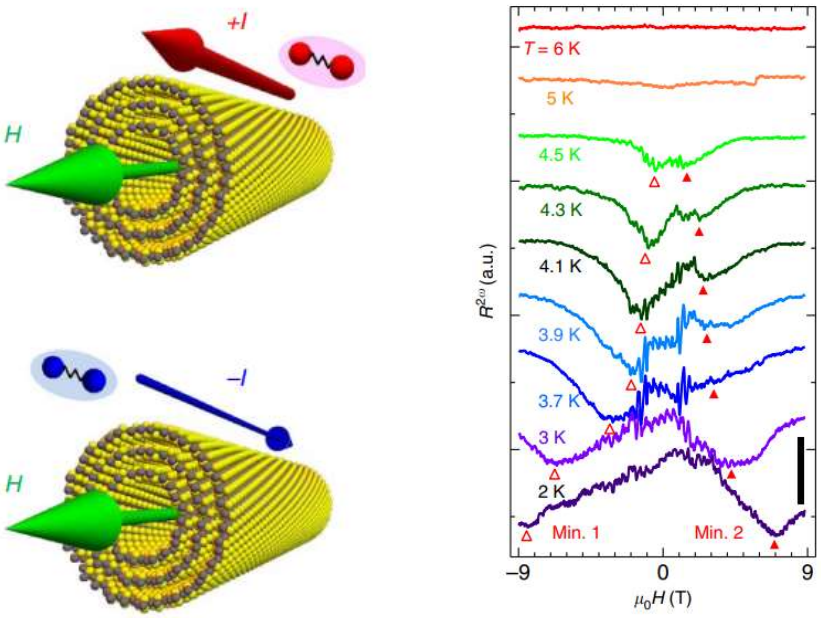

Fig. 1-7-1 Schematics of unidirectional electric transport in a tungsten disulfide nanotube.

The magnitude of magnetoresistance was asymmetric when the electric current was applied to nanotube-shaped tungsten disulfide under the magnetic field.

1-8 Superconductivity under Magnetic Field

In systems where superconductivity and a magnetic field exist, the surface energy follows the equation: $E = \frac{{H_c}^2(\xi-\lambda)}{8\pi}$, where ξ is a coherence length, λ is a London penetration length, and $\frac{{H_c}^2}{8\pi}$ is gap energy between superconductivity and normal conductivity. The surface energy is determined by the competition of ξ and λ. Superconductor is classified into two types with a magnetic field (Fig. 1-8-1). Given that $\xi > \lambda$, this system is Type I superconductor, where expels magnetic fluxes to maintain superconductivity. With a magnetic flux penetration, superconducting state is immediately destroyed. Examples of type I superconductors are Aluminum and lead. Given that $\xi < \lambda$, this system is Type II superconductor. it retains a mixed state where a magnetic flux is divided as finely as possible and enters the inside of the superconductor. Examples of type II superconductors are alloys and organic materials such as Nb_3Ge[18] and κ-$(BEDT\text{-}TTF)_2 \cdot Cu(NCS)_2$[19].

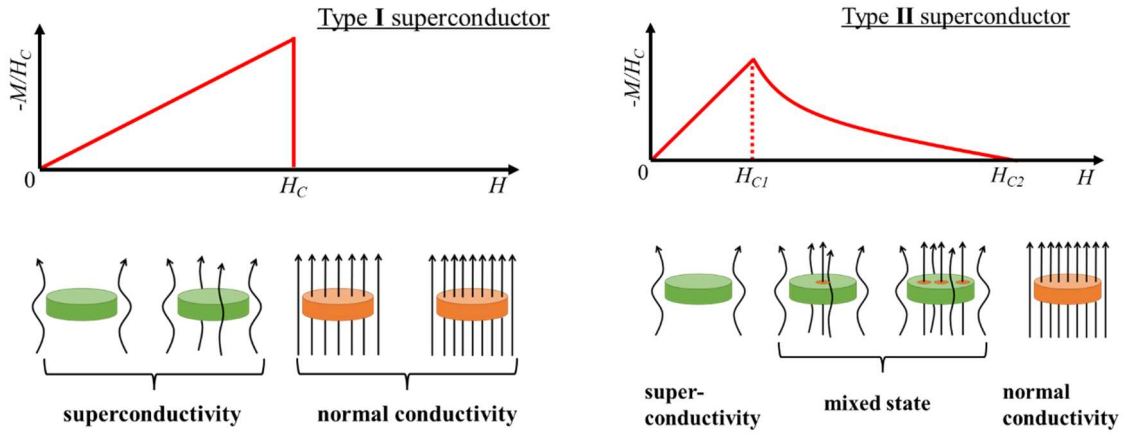

Fig. 1-8-1 Magnetization process of type I / II superconductors. Whereas a type I superconductor expels magnetic fluxes, a type I superconductor retains magnetic fluxes in itself.

1-9 Bogoliubov Quasiparticles

In a process of forming Cooper pairs at a superconducting transition, a large number of electrons near the Fermi surface collapses into and occupy the lowest state. Superpositions of excitations of negatively charged electrons and positively charged electron holes construct quasiparticles, which are called Bogoliubov quasiparticles[20]. This can be viewed as superpositions of electron pair and hole pair, thus Bogoliubov quasiparticle has $s = \frac{1}{2}$ (Fig. 1-9-1).

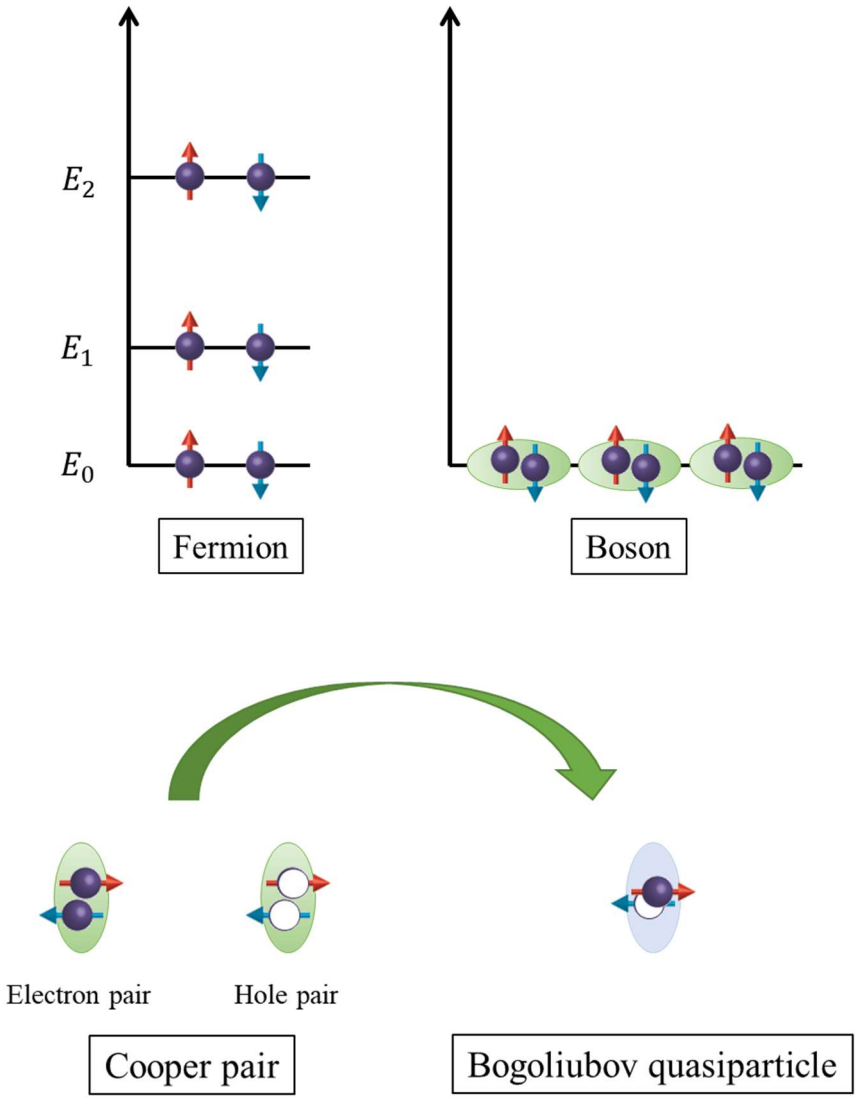

Fig. 1-9-1 Fermions follow the Hund's rule and exclusion principle, where particles fill

states from the bottom of the energy order, while bosons allow particles with the same quantum number to occupy the same state. In the superconducting state, fermionic electrons are condensed to a lower energy order immediately because of Cooper pairs, which are bosons.

The state is excited by an electron-hole pair at the transition temperature.

1-10 Molecular Conductor

A molecular material can be a conductor by forming the electronic band and generating the carrier. Many molecular conductors have been synthesized with tetrathiafulvalene (TTF), where abundant π electrons exist. TTF can be stuck densely due to the planarity and is very stable for oxidation. TTF-TCNQ is a typical molecular metal with 1D conducting chain and is unstable in a low temperature, where Peierls transition occurs[21]. To expand the dimension of the conducting pass, BEDT-TTF was synthesized. Two six-membered rings were adopted to each terminal of TTF. Various physical properties in molecular conductors have been achieved by replacing the counter anions and by synthesizing BEDT-TTF derivatives. Several BEDT-TTF salt exhibits superconductivity[22] (Fig. 1-10-1).

κ-$(BEDT\text{-}TTF)_2 \cdot Cu(NCS)_2$ (hereafter, κ-NCS) exhibits superconductivity after a Mott transition where the bulk superconducting transition temperature is 10.4 K[19]. This crystal is composed of the cation radical of BEDT-TTF and its counter anion $Cu(NCS)_2$. BEDT-TTF molecules form dimers carrying +1 hole, which can express as a strongly correlated electron system. One dimer of BEDT-TTF is almost perpendicular to the other dimer of BEDT-TTF, forming a κ-type arrangement (Fig. 1-10-2). The conducting pass is spread two dimensionally, which is divided by $Cu(NCS)_2$. Both constituent molecules are achiral. However, a relative configuration of these two molecules results in a chiral structure. This material has a non-centrosymmetric space group $P2_1$ of which 2_1 screw axis runs along the b-axis. According to electron diffraction experiments of the thin crystal, d-form systems are often obtained[23].

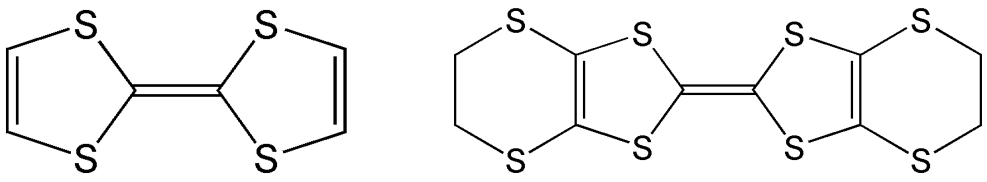

Fig. 1-10-1 The molecular structures of TTF and BEDT-TTF

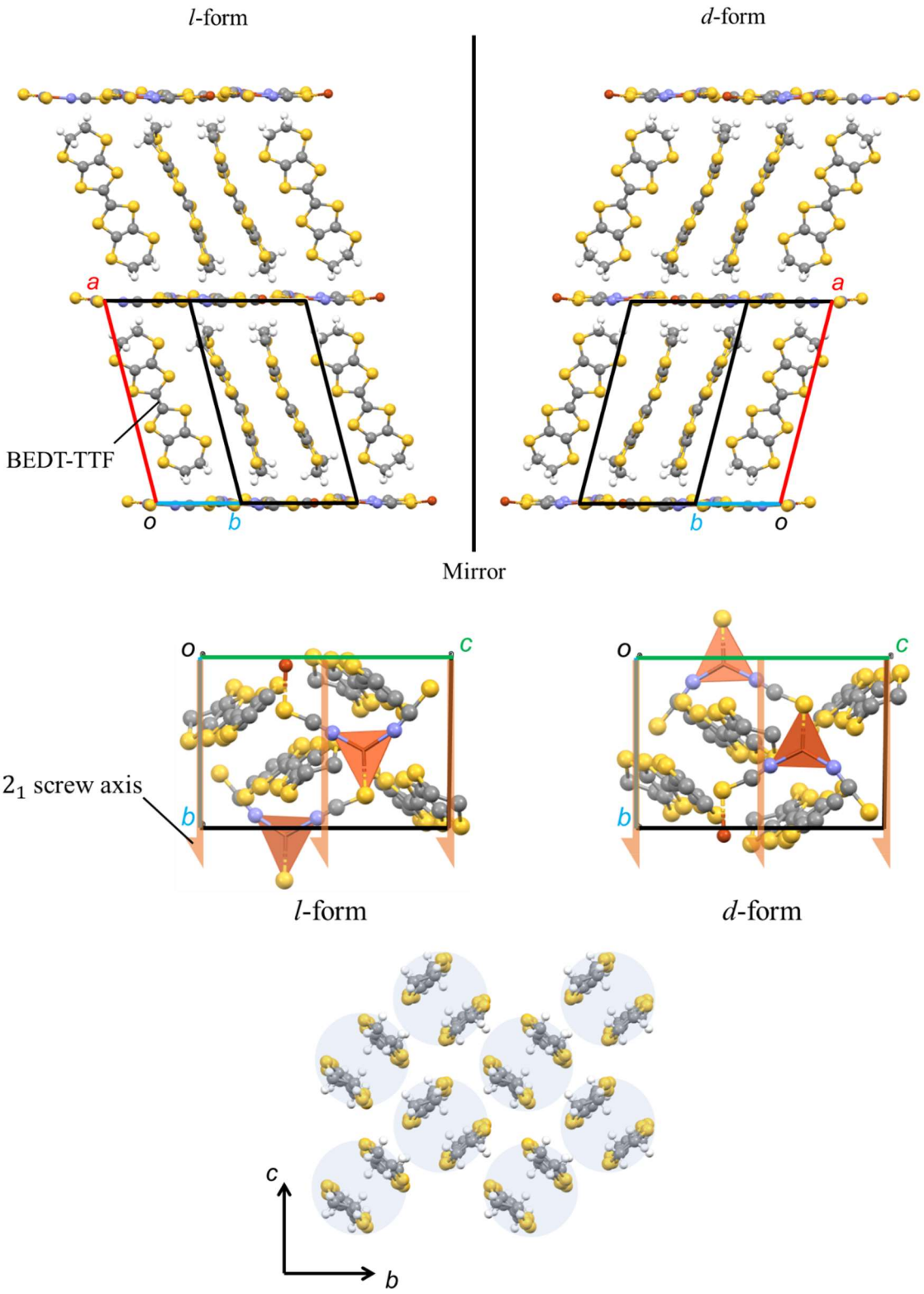

Fig. 1-10-2 The crystal structures of d-form and l-form in κ-NCS.

The conducting pass, forming a κ-type arrangement.

1-11 Mott Insulator

The electron/lattice density ratio also governs a physical property in a solid state. If the ratio is a simple integer, electrons are localized along with a certain pattern to elude Coulomb repulsion[24] (Fig. 1-11-1). The electron wavefunction gains kinetic energy when it is as broad as possible. However, when the Coulomb repulsion is sufficiently large compared to the electron kinetic energy, the stabilization energy due to localization become dominant and the conduction electrons become insulating. Mott insulators are systems, where the electron/lattice density ratio is an integer ratio of 1:1, and many compounds have this Mott insulating state. The phase transition from Mott insulator to metal is called the Mott transition. Mott transitions can also occur by doping carriers to control band filling, or by compressing the lattice to increase the kinetic energy of the electrons. Accordingly, some Mott insulators have a superconducting phase including κ-NCS in the vicinity of the Mott insulating state.

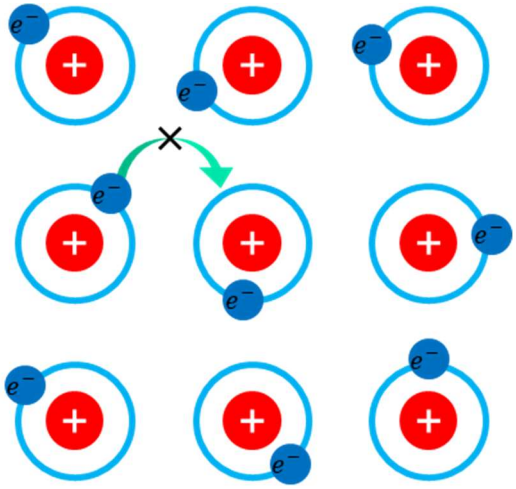

Fig. 1-11-1 Schematic of Mott-insulator. Electrons cannot move owing to Coulomb repulsion.

1-12 Determination of Absolute Configuration in X-ray crystallography

The composite amplitude and phase of X-ray waves scattered from all atoms in one unit cell are given by the structure factor: $F(hkl) = \sum_{j=1}^{N} f_j \, exp\{2\pi i(hx_j + ky_j + lz_j)\}$, where f_j is an atomic scattering factor, x_j, y_j, and z_j are coordinates of each, and h, k, l are mirror indexes of each. The diffraction intensity $I(hkl)$ of hkl is proportional to the square of the structure factor, $I(hkl) = I(\bar{h}\bar{k}\bar{l})$. Thus, it means that in any crystal, the reflection intensity from a certain plane and its backside are equal. This is called Friedel's law.

However, part of the incident X-ray is absorbed by the source material when the wavelength of the incident X-ray is at the absorption edge. This is called anomalous scattering. The effect of absorption incorporates an imaginary term into an atomic scattering factor derived from amplitude changes. A new structure factor is given by the following equation: $F(hkl) = (f'_M + if''_M) \, exp\{2\pi i(hx_M + ky_M + lz_M)\} + \sum' f_j \, exp\{2\pi i(hx_j + ky_j + lz_j)\}$. Here, x_M, y_M, and z_M are the coordinates of the M atom, and $\sum'$ means that the term for $j = M$ is excluded. Thus, $I(hkl) \neq I(\bar{h}\bar{k}\bar{l})$. With anomalous scattering, an absolute configuration in a single crystal is determined[25].

To identify handedness of a bulk crystal, X-ray irradiated several points of the single crystal. Flack parameter estimates quantity of an absolute configuration. This is calculated by the following equation: $I(hkl) = (1 - x)|F(hkl)|^2 + x|F(-h - k - l)|^2$, where x is a value of a Flack parameter. Here, x is found between 0 to 1. If x is 0, the crystal is correct and shows enantiopure. If x is 1, the inverted structure is correct. If x is near 0.5, it is racemic.

1-13 Time-reversal Symmetry

Physical phenomena can be mathematically characterized by elucidating features of a system that are conserved under certain operations as symmetry. Chirality is understood as a form in which itself and its mirror image do not overlap. In terms of symmetry, it is a form in which spatial inversion symmetry is broken. A similar argument can be made for time, where reversal of time direction reproduces a real-world phenomenon. Time-reversal symmetry means that physical laws remain invariant when $t \to -t$. For example, $\boldsymbol{v}(t) \to -\boldsymbol{v}(-t), \boldsymbol{B}(t) \to -\boldsymbol{B}(-t), \boldsymbol{F}(t) \to \boldsymbol{F}(-t)$, where velocity, magnetic field, and force, respectively. T-odd is defined to be sign-inverted under time-reversal operation and T-even to be not. Thus, $\boldsymbol{v}$, $\boldsymbol{B} = T$-odd, $\boldsymbol{F}, = T$-even. Considering that mass (m) is zeroth-order with respect to time, $m = T$-even.

In quantum mechanics, the solution under time-reversal operation of the Schrödinger equation: $i\hbar\frac{\partial}{\partial t}\Psi(\boldsymbol{x},t) = \left[-\frac{\hbar^2}{2m}\boldsymbol{\nabla}^2 + \boldsymbol{V}(\boldsymbol{x})\right]\Psi(\boldsymbol{x},t)$, whose left-hand side is sign-reversed by the energy operator $i\hbar\frac{\partial}{\partial t}$, is solved by considering the wavefunction Ψ to change into a complex conjugate Ψ^*. In other words, this energy term of the Schrödinger equation is also T-even.

$$i\hbar\frac{\partial}{\partial t}\Psi(\boldsymbol{x},t) = \left[-\frac{\hbar^2}{2m}\boldsymbol{\nabla}^2 + \boldsymbol{V}(\boldsymbol{x})\right]\Psi(\boldsymbol{x},t).$$

By applying $t \to -t$,

$$-i\hbar\frac{\partial}{\partial t}\Psi(\boldsymbol{x},-t) = \left[-\frac{\hbar^2}{2m}\boldsymbol{\nabla}^2 + \boldsymbol{V}(\boldsymbol{x})\right]\Psi(\boldsymbol{x},-t).$$

By taking the complex conjugate,

$$i\hbar\frac{\partial}{\partial t}\Psi^*(\boldsymbol{x},-t) = \left[-\frac{\hbar^2}{2m}\boldsymbol{\nabla}^2 + \boldsymbol{V}(\boldsymbol{x})\right]\Psi^*(\boldsymbol{x},-t).$$

Thus, both $\Psi(\boldsymbol{x},t)$ and $\Psi^*(\boldsymbol{x},-t)$ satisfy the same equation.

§2 CISS effect in chiral molecular superconductor

2-1 Introduction and Experimental Design

The author has focused the attention on a chiral superconductor to further enhance the CISS effect presumably due to its coherent nature that can enhance the spin diffusion length. Macroscopic coherence of the superconducting state may also enable spatial mapping of spin accumulation. In order to achieve spin generation by a chiral superconductor, the author has selected κ-NCS. This material is a chiral molecular superconductor with T_c = 10.4 K and a non-inversion symmetrical space group.

The author has elucidated handedness distribution in bulk κ-NCS single crystals by using single crystal X-ray diffraction. Magnetic electrodes are required for the observation of a spin-dependent transport phenomenon. In the CISS effect, the application of a current to a chiral material causes spin polarization, which would be observed as magnetoresistance by detecting the spin with a magnetized electrode (Fig. 2-1-1). These electrodes and arrangements have been adopted by device fabrication process. Although d-form systems are often obtained in thin crystals, the author also prepared bulk crystals to investigate the handedness distribution in a more crystal-grown crystal.

Superconducting CISS effect was demonstrated by detecting a voltage drop (V) generated at the interface between κ-NCS and a nickel electrode with an a.c. electric current (I_{ac}). When an electron passing through the chiral superconductor flows into the electrode, it carries spin polarization generated by CISS effect. Once the up-spin current enters the electrode, excess of up-spins appears at the interface. Hence, the polarity of the spin accumulation is up-spin in the electrode. Reversing the electron flow doesn't change the polarity of interfacial spin accumulation because down-spins are removed from the electrode. Such spin polarization under a.c. excitation by I_{ac} produces d.c. V at the interface on time average. The voltage sign depends on a relative angle between the spin accumulation polarity and the magnetization of the ferromagnetic nickel electrode. The d.c. V is derived from the electrochemical potential shift. In terms of quantum mechanics, the definition of the direction of spin is opposite from the one of magnetization. Given that Ni is magnetized downward, the majority spin is up-spin in the bulk. However, the majority spin at the Fermi surface is opposite from the one in the bulk in Nickel. The down-spin is major at the Fermi surface. The chemical potential of the down-spin decreased with the up-spin injection due to the charge neutrality condition.

The value of the shift in the down-spin is smaller compared to that of the up-spin following the equation: $\mu_\sigma = -e\phi + \frac{\delta n_\sigma}{N_\sigma}$, where μ_σ is the electrochemical potential, n_σ is the spin density at the Fermi surface, N_σ is the density of state at the Fermi surface. The entire electrical potential is shifted to the down-spin side. When the minus terminal of the voltmeter is connected to the Ni electrode, the plus voltage appears. In this case, the generated spins and the Ni magnetization is antiparallel with plus voltage: it is parallel with minus voltage (Fig. 2-1-2).

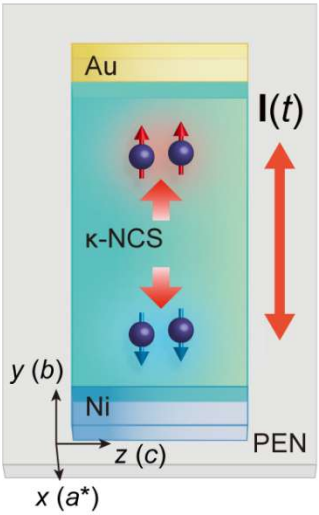

Fig. 2-1-1 Schematic of κ-NCS device. $I(t)$ is an electric current.

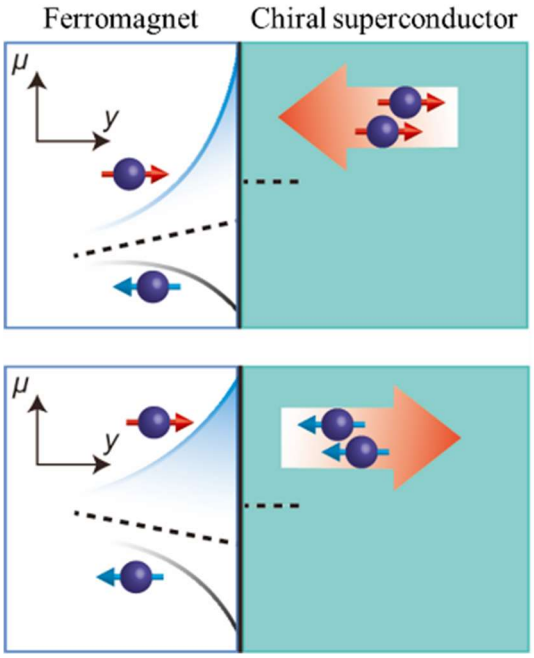

Fig. 2-1-2 Electrochemical potential diagram at the junction between a chiral superconductor and ferromagnet. An a.c. electric current produces a d.c. spin-dependent voltage drop on time average.

2-2 Experiments

2-2-1 Material Preparation

Bulk crystals (bulk #1) of κ-NCS were obtained following the previous report[19]. BEDT-TTF (20 mg, 0.052 mmol), TPP·SCN (80 mg, 0.20 mmol), and Cu·SCN (20 mg, 0.20 mmol) were added to a mixed solution of 1,1,2-trichloroethane +10% (v／v) ethanol (60 mL) in H-shaped cell with Pt electrodes under an Ar atmosphere. 1,1,2-trichloroethane +10% (v／v) ethanol was dried with sodium sulfate in advance. Hexagonal black crystals were obtained after applying a constant current of 1.0 μA for 24 hours at 30℃. As the other method, bulk crystals (bulk #2) of κ-NCS were synthesized with chlorobenzene (35 mL), methanol (15 mL) and 1,1,2-trichloroethane +20% (v／v) methanol (10 mL) instead of 1,1,2-trichloroethane +10% (v／v) ethanol (60 mL).

Thin crystals of κ-NCS were obtained following the previous report. BEDT-TTF (20 mg,0.052 mmol), TPP·SCN (80 mg,0.20 mmol), and Cu·SCN (20 mg,0.20 mmol) were added to a mixed solution of chlorobenzene (35 mL), methanol (15 mL) and 1,1,2-trichloroethane +20% (v／v) methanol (10 mL) in two of each flat bowl-shaped vessel with Pt electrodes under an Ar atmosphere. Dark brown thin crystals were obtained after applying a constant current of 3.5 μA for 15 hours at 30℃. Thin crystal of κ-NCS was laminated onto a PEN (polyethylene naphthalate) substrate by using a strand of hair in isopropanol after having been rinsed by 1,1,2-trichloroethane +20% (v／v) methanol following isopropanol. Photolithography method prepared PEN substrates where Au and Ni electrode (Thickness ≈ 33 nm) were evaporated. Ni electrodes were capped by thin Au (Thickness ≈ 3 nm) to prevent from oxidation by air. Three devices (device #0, device #1, device #2) were fabricated by Au wire and Ag paste.

2-2-2 Circular Dichroism Microscopy

Circular dichroism measurement revealed handedness distribution of two thin crystals. A photoelastic modulator can produce circularly polarized light in commercial CD spectrometer. But appearance of linear polarization components is inevitable between continuous right (RCP) and left circular polarization (LCP) (Fig. 2-2-2-1). This linear polarization wave changes circularly polarized light through a crystal without relation to its chirality. In order to irradiate RCP/LCP to a crystal respectively, vertically polarized beams and horizontally polarized beams were divided by a beam displacer in advance and were alternately delivered by a rotatory chopper. After being recombined by another beam displacer, a quarter waveplate modulated these two beams into RCP/LCP depending on its polarization angle. By irradiating modulated circularly polarized light to a chiral crystal, the difference of the absorbance was observed[26]. The CD signal is given by $\frac{I_L - I_R}{I_{L0} + I_{R0}} \times 100$, where $I_{L/R}$ is the magnitude of left-/right-handed circularly polarized light. $I_{L0/R0}$ is the reference magnitude of a left-/right-handed circularly polarized light transmitted only through the substrate.

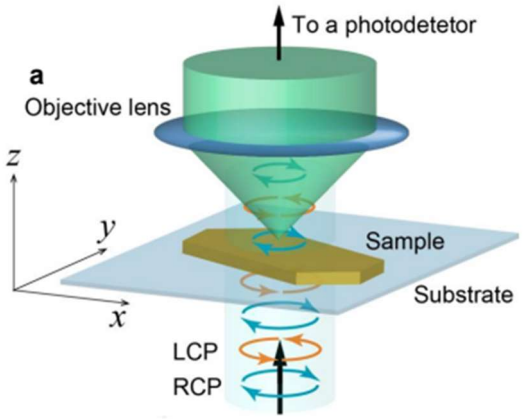

Fig. 2-2-2-1 Schematic of the experimental geometry for CD microscopy.

In device #1, the CD measurement showed the intensity over the entire area and revealed that the crystal carried a spatially uniform enantiomeric excess (Fig. 2-2-2-2).

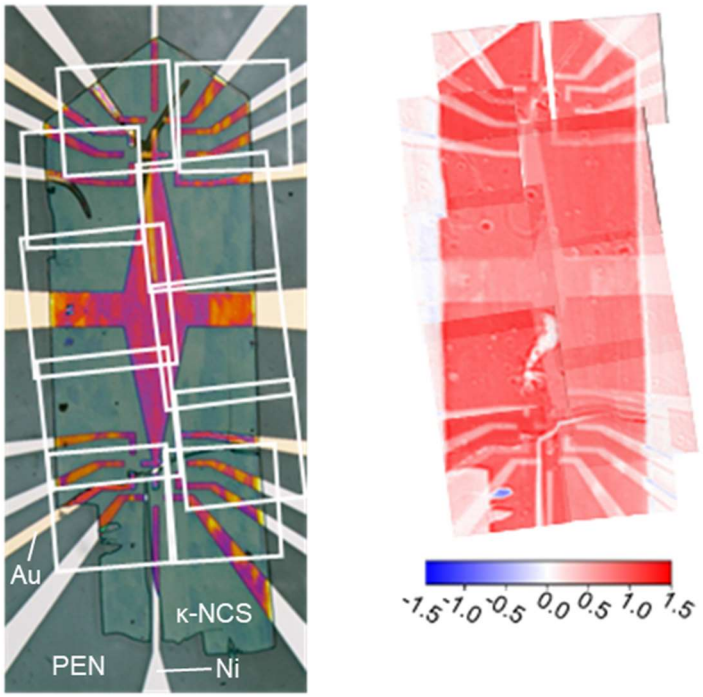

Fig. 2-2-2-2 CD microscopy of device #1. The images were taken at room temperature. the CD signal was evaluated using the modulation of circularly polarizes light. The uniform sign of the CD signal confirmed the uniform enantiomeric excess of the thin κ-NCS device except for the electrodes.

In device #2, the CD measurement revealed that two domains of opposite handedness coexist (Fig. 2-2-2-3). Each two excitation electrodes pairs were arranged in the opposite handedness domains. Area A was on the blue CD region, where the handedness was opposite from device #1. Area B was on the red CD region, where the handedness was identical to device #1 and opposite from Area A (Fig. 2-2-2-4).

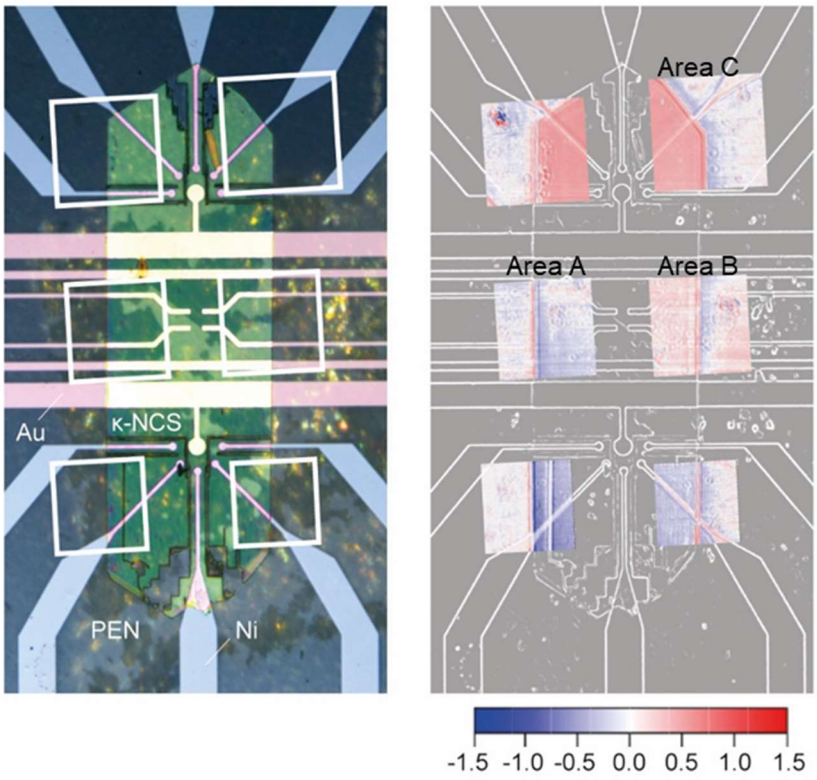

Fig. 2-2-2-3 Microscopic image and CD microscopy of device #2. CD microscopy was repeatedly performed on each white square. The sign of CD signals of κ-NCS changed around the center. The lower domain in blue has the opposite handedness to device #1, while the upper domain in red has the same handedness.

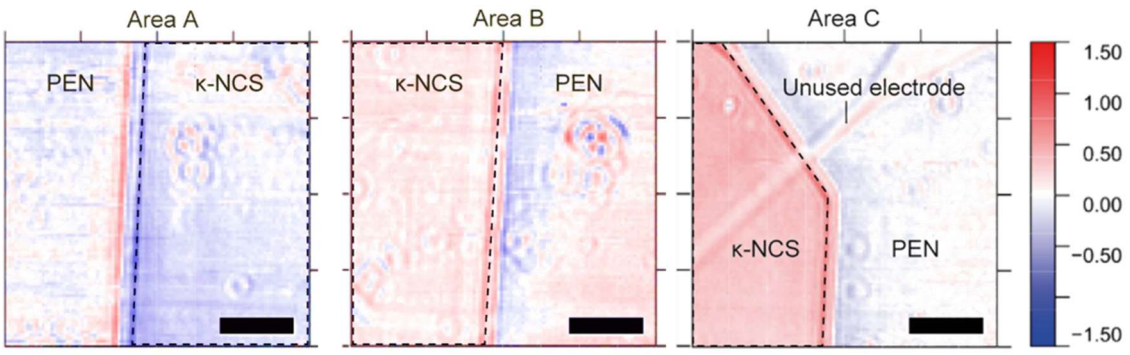

Fig. 2-2-2-4 CD microscopy at each area. Area A showed the blue domain of κ-NCS. Area B and Area C showed the red domains of κ-NCS.

Regarding the synthesis of thin films of κ-NCS, handedness is determined incidentally. However, more thin films with a red signal in the CD measurement were obtained (Fig. 2-2-2-5).

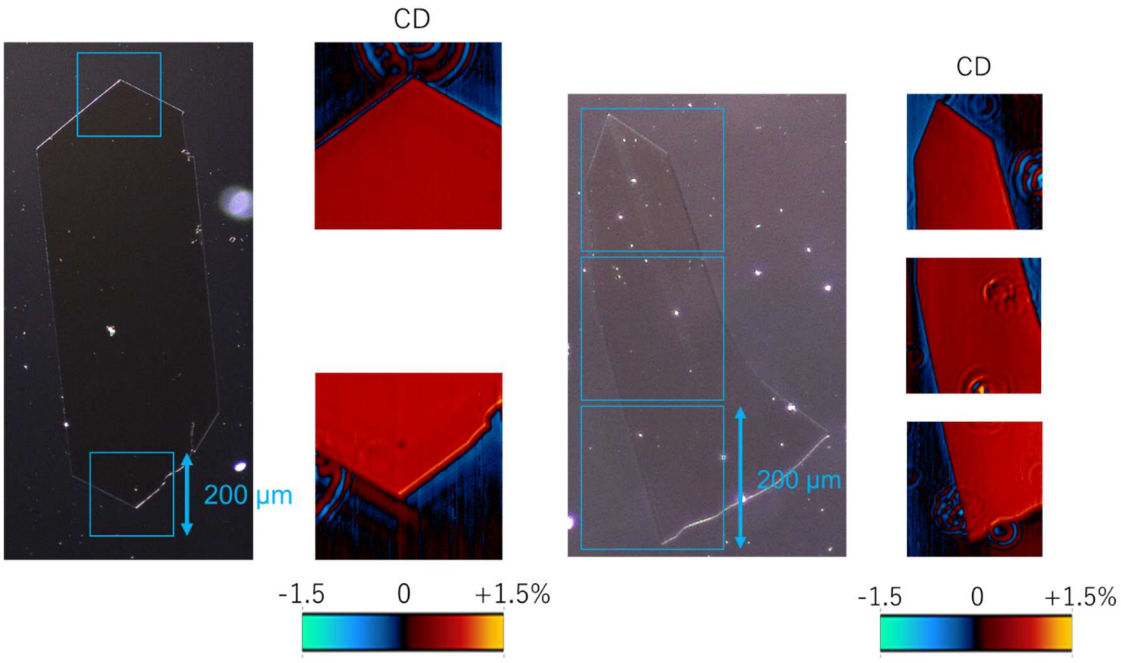

Fig. 2-2-2-5 CD microscopy of other κ-NCS thin crystals.

2-2-3 Characterization of Bulk Crystals

X-ray diffraction can determine the handedness of crystals by calculating the so-called Flack parameter. This is a strong tool to determine the absolute chiral structure which is difficult to achieve unless CD spectra are obtained. Flack parameter is even stronger than CD because it can determine the absolute structure.

X-ray irradiated three regions of the single bulk #1 crystal (Length ≈ 0.23 mm) (Fig. 2-2-3-1). In the top of the crystal, the handedness was right and its Flack parameter was 0.090. In the bottom of the crystal, the handedness was left and its Flack parameter was 0.050. The handedness in one side of the crystal was opposite of the handedness in the other side of the crystal. The bulk #2 crystal was larger than the bulk #1 crystal and enabled to measure the handedness specification finely. This measurement provided the similar results. The Flack parameter had a smaller value toward the edge of the crystal, indicating that one side had more degree of chirality (Fig. 2-2-3-2). From these facts, it was predicted that the crystal grew from the edge and the handedness was inverted during the growth. As X-ray absorption varies depending on the shape of the single crystal, the measurements were also made with the crystals mounted upside down. Nevertheless, the handedness distributions in the crystals were the same, respectively.

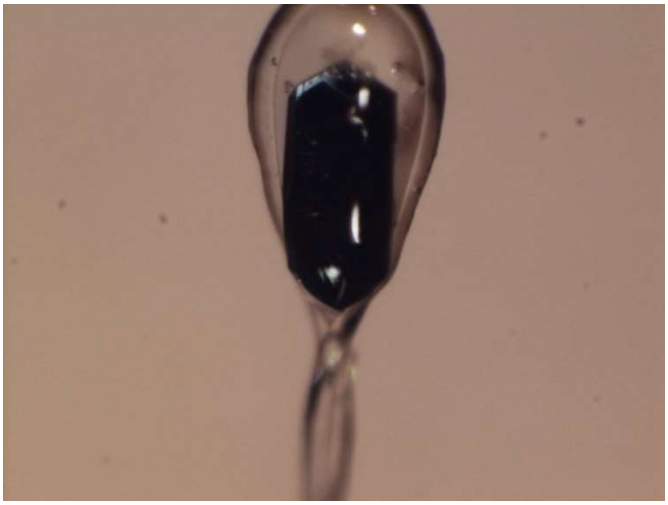

Fig. 2-2-3-1 Bulk crystal of κ-NCS.

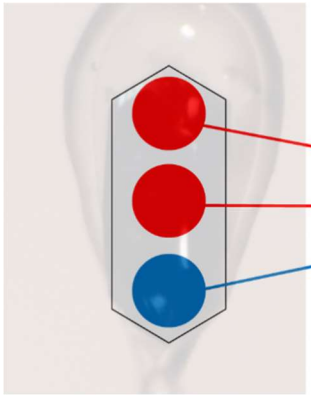

Flack parameter	Major handedness
0.090(18)	Right
0.125(11)	Right
0.050(6)	Left

Bulk #1

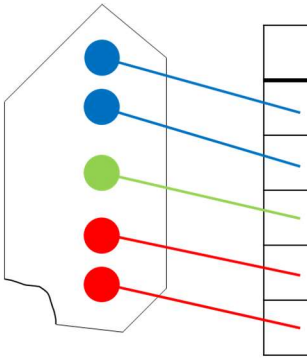

Flack parameter	Major handedness
0.239(9)	Left
0.350(9)	Left
0.457(8)	Racemic mixture
0.373(11)	Right
0.360(13)	Right

Bulk #2

Fig. 2-2-3-2 Flak parameter and handedness distribution in κ-NCS.

2-2-4 Electrical Measurements in Device #0

Having been attached to the soft PEN substrate, the thin crystal was subjected to compressive strain. The electrical measurements were made to confirm that the superconducting transition would indeed undergo with an electric current of 1 μA.

In devices #0, The electrical measurement was performed with the standard four-probe method from 300 K to 2 K (Fig. 2-2-4-1). the electrical resistance was decreased from room temperature and showed a phase transition to the semiconductor around 175 K. This semiconducting behavior derived from Mott transition. From 50 K, the resistance exhibited metallic behavior and vanished sharply at 7.5 K. This absence of the resistance was the superconducting transition. This transition temperature (T_c) was defined as the middle of the transition and was lower than that of the bulk crystal because of the compressive strain from the PEN substrate. With this device, the resistance slightly increased to 0.5 Ω after zero resistance (Fig. 2-2-4-2). This resistance was caused by a small fraction of the superconducting state.

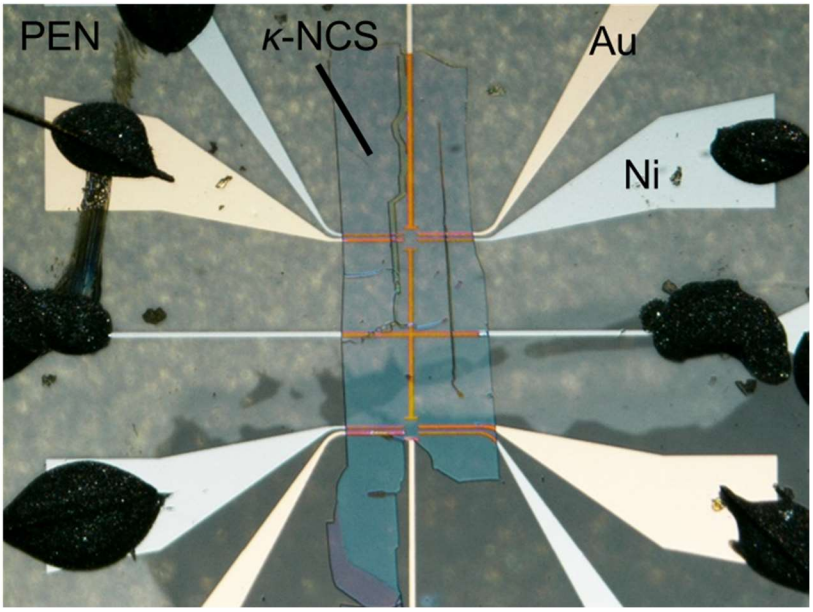

Fig. 2-2-4-1 Macroscopic image of device #0.

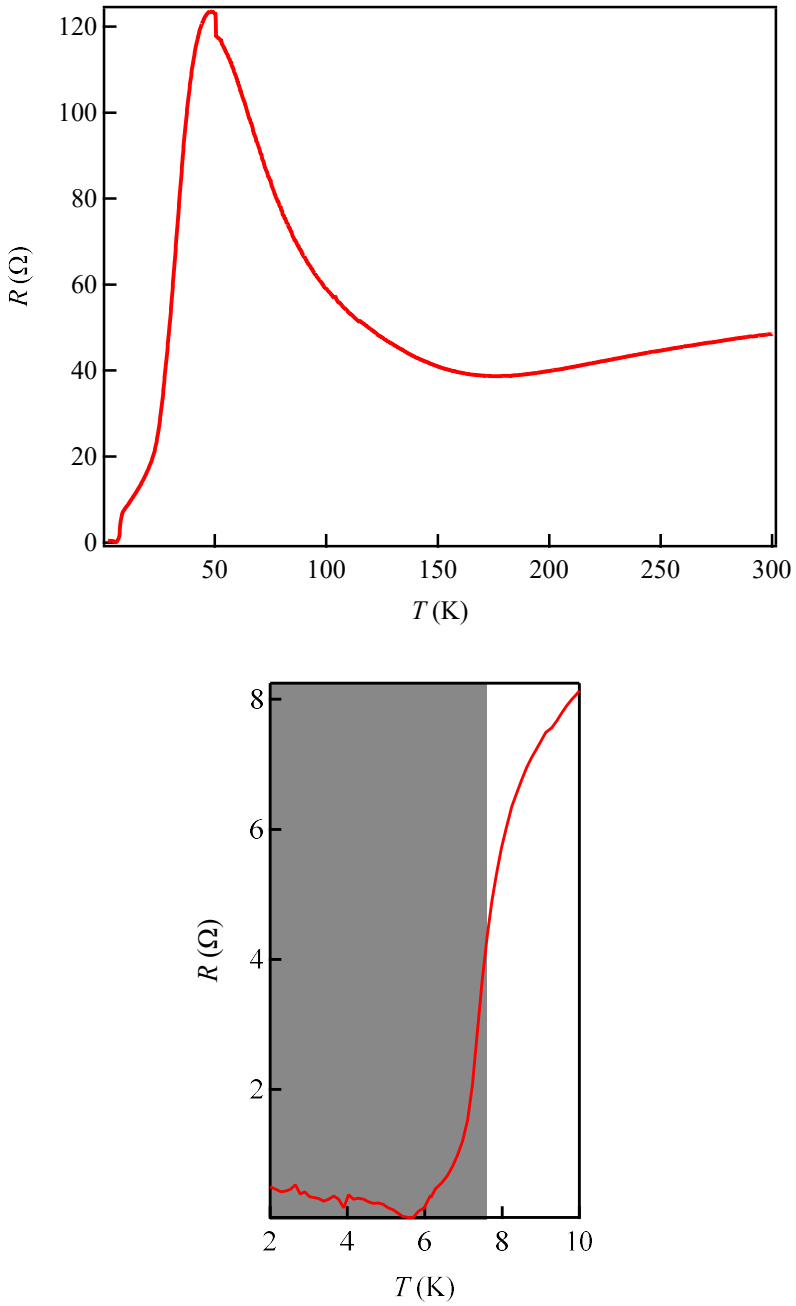

Fig. 2-2-4-2 Temperature dependence of resistance. T_c = 7.5 K.

In order to detect spin polarization, the magnetoresistance (MR) measurement is one of the strongest methods in spintronics. To begin with, the author has started a standard four-probe measurements with κ-NCS device comprising Au/Ni electrodes. The reason why the author used Au/Ni is to detect spins as a magnetoresistance.

At first, a d.c. electric current (I) was applied to this device under the magnetic field at 5.6 K where the resistance was mostly reach zero. When an electric current of +0.2 μA was applied from the Ni electrode to the Au electrode with the parallel magnetic field, the resistance (R) was increased by applying the magnetic field. The resistance was saturated around -10 kOe although it was increased linearly around +10 kOe. The smallest resistance was obtained in the positive magnetic field region. However, this asymmetric behavior was inverted with an electric current of -0.2 μA. When an electric current of 0.4 μA was applied, the resistance was not saturated at -10 kOe. The asymmetricity was suppressed by adding more currents (~2.0 μA) (Fig. 2-2-4-3).

$R_{odd} = [R(+10\ \mathrm{kOe}) - R(-10\ \mathrm{kOe})]/2$ was defined for quantitative analysis. R_{odd} was decreased by applying the larger electric currents. If the difference in MR is caused by spin accumulation, the difference in MR should have increased as the current increased. In reality, the antisymmetric component of the graph was larger when the applied current was smaller. Critically, such a voltage signal appeared even without applying a current to the sample.

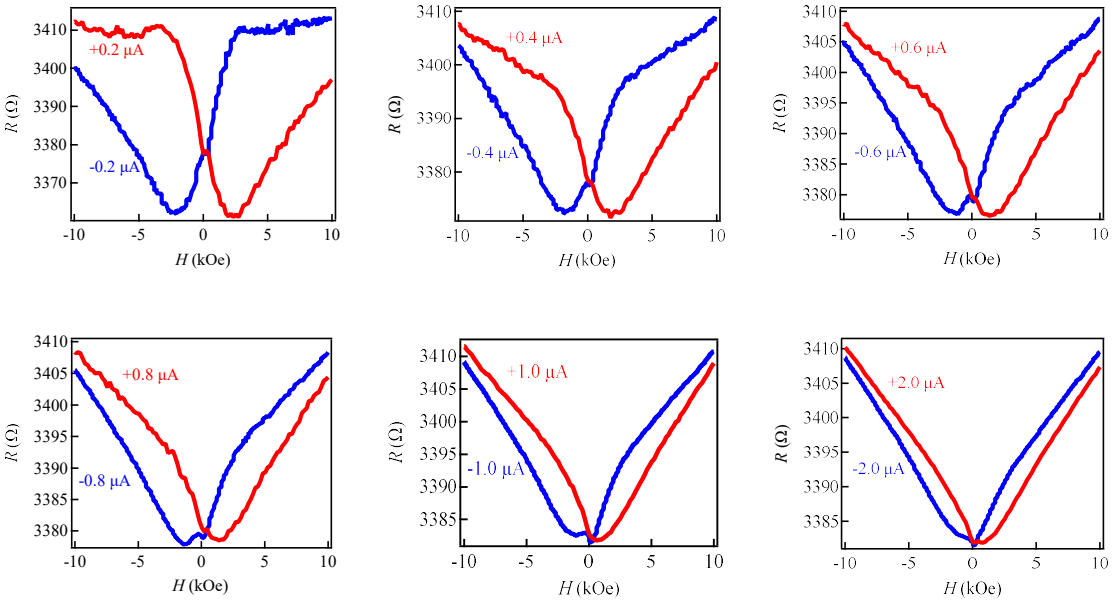

Fig. 2-2-4-3 Magnetic field dependence of resistance with d.c. electric currents, which suppressed asymmetry of resistance.

Voltaic effect rather than magnetoresistance was accidentally observed by applying a d.c. electric current (Fig. 2-2-4-4). The reason why signal was observed even under 0 μA was due to noise in the laboratory. In fact, when the measurement system was shielded with aluminum foil, no signal appeared. It was desired to supply an a.c. electric current instead of noise for further investigation.

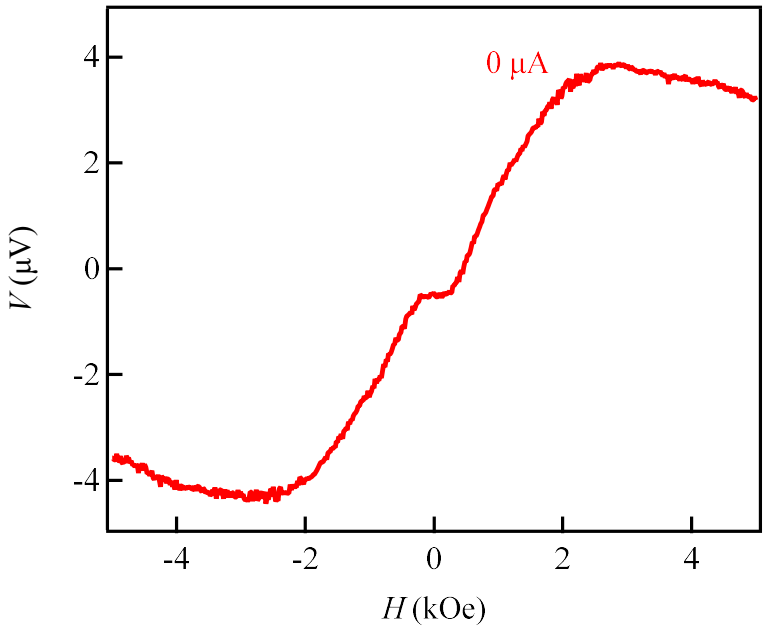

Fig. 2-2-4-4 Magnetic field dependence of voltage without electric currents.

2-2-5 Electrical Measurements in Device #1

Device #1 was designed to investigate this voltage drop at κ-NCS/Au/Ni interface more carefully.

The electrical measurement was performed with the standard four-probe method from 300 K to 2 K with an electric current of 10 μA. The electrical resistance was increased from room temperature to 100 K after short metallic behavior around 300 K. This semiconducting behavior derived from Mott transition. From 100 K, the resistance exhibited metallic behavior and the device underwent the superconducting transition. It showed that T_c was 7.5 K. A temperature-dependent difference in the thermal expansion coefficients of the substrate and κ-NCS caused the anomaly behavior around 20 K. With this device, the resistance never reached zero after the superconducting transition. This residual resistance was caused by a small fraction of the superconducting state (Fig. 2-2-5-1). However, the residual resistance was suppressed by annealing at the glass transition temperature (80 K), where terminal ethylene groups of BEDT-TTF tend to be regularly structured.

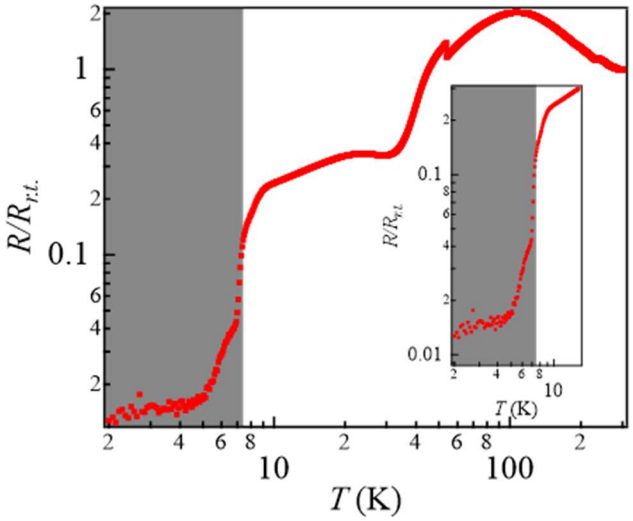

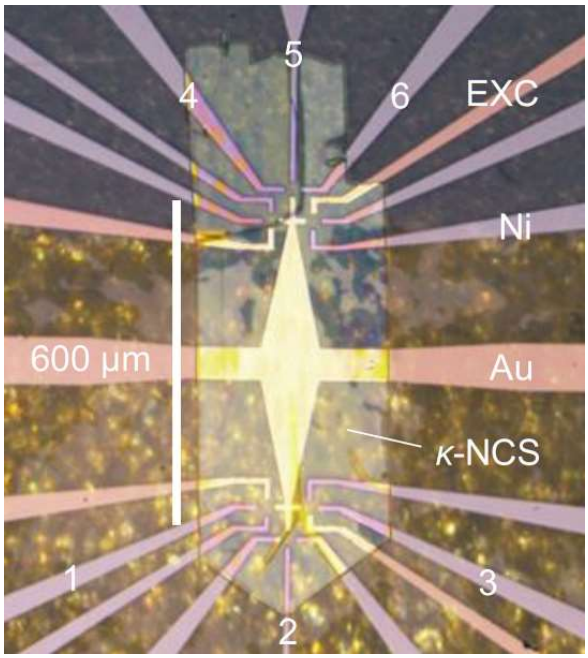

Fig. 2-2-5-1 Temperature dependence of resistance in device #1, where $T_c = 7.5\,K$ and microscopic image of device #1.

An a.c. electric current (I_{ac}) was applied between the Ni electrode and the Au electrode under the magnetic field at 7.5 K. In practice, I_{ac} was applied to the entire circuit, and the circuit was designed to measure the shift in the chemical potential created at the interface between κ-NCS and the Ni electrode via a capacitance connected in parallel with a voltmeter. The input electric current was generated by AC power supply. When I_{ac} was off, voltage (V) did not appear. Upon the application of I_{ac}, V appeared and was increased by increasing I_{ac} (~ 6.0 μA). V reversed sign upon the reversal magnetic field $(\boldsymbol{H})$ direction and exhibited the nonlinear field dependence. Moreover, $V_{odd} = [V(+5\ \mathrm{kOe}) - V(-5\ \mathrm{kOe})]/2$ was defined for quantitative analysis. V_{odd} showed that asymmetry of voltage was increased by increasing I_{ac} (Fig. 2-2-5-2).

The author investigated the magnetic field dependence of Ni substrate where electrodes patterns had been drawn by using a superconducting quantum interference device magnetometer, MPMS-XL7 (Quantum Design). The magnetization of the Ni electrode exhibited the similar field dependence (Fig. 2-2-5-3). $\boldsymbol{H}$ dependence of V confirmed

that it surely corresponded to the magnetization curve of nickel, which means that V originates in the interfacial spin accumulation.

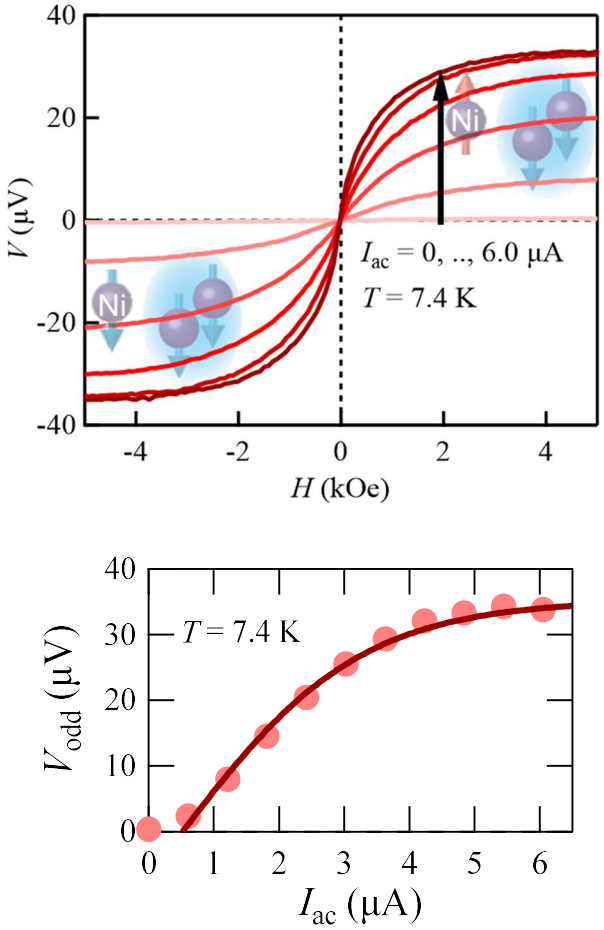

Fig. 2-2-5-2 Magnetic field dependence of voltage with a.c. electric currents increased and an electric current dependence of V_{odd}. Upon the application of a.c. electric current, large spin-dependent voltage appeared. The voltage sign depends on a relative angle between the spin accumulation polarity and the magnetization of Ni electrode.

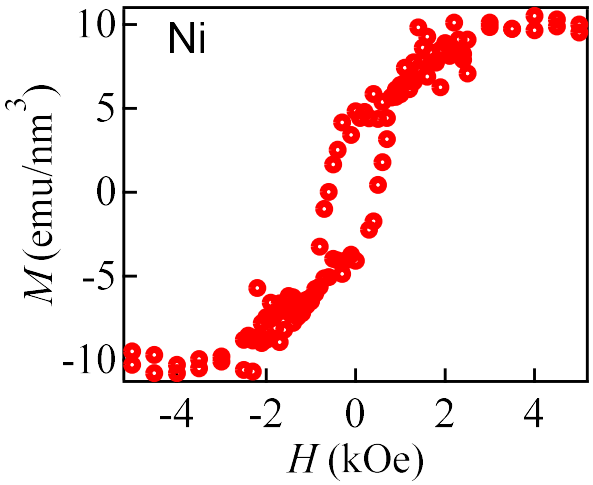

Fig. 2-2-5-3 Magnetization curve of the Ni electrode. The Ni electrode exhibited the similar field dependence. The correspondences showed that voltage signal was affected by the spin polarization direction in the Ni electrode.

The angle (θ) dependence of H within the crystal plane from the y-axis determined the direction of the spin polarity $(\boldsymbol{\sigma})$. I_{ac} was applied to each hetero terminal. The input electric current was generated by AC power supply of setting to 100 $mV_{p\text{-}p}$. When $\boldsymbol{H}$ was reversed, the detected voltage was also reversed, and an antisymmetric field dependence appeared (Fig. 2-2-5-4).

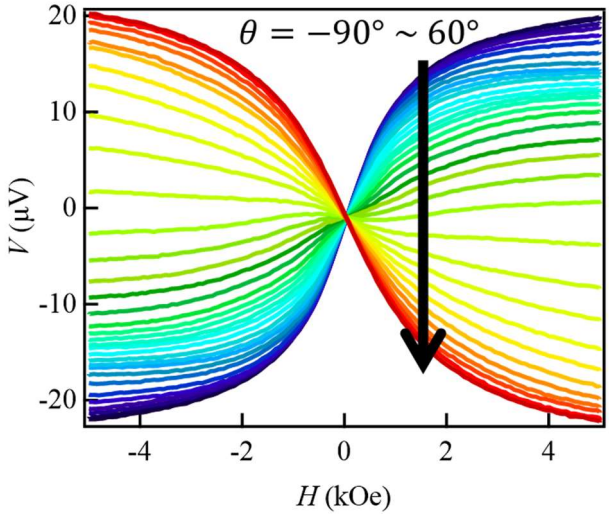

Fig. 2-2-5-4 Magnetic field dependence of voltage at different angle values at intervals of 5 degrees.

Supposing that the superconducting state collapses by the magnetic field, V would be observed also. In order to preclude possible resistance generation by superconducting state suppression, the author has investigated the stability of the superconducting state under a magnetic field. The electrical measurement under 10 kOe along the y-axis was performed. The same superconducting transition was exhibited as for the zero magnetic field measurement (Fig. 2-2-5-5). This means that the superconductivity survived up to 10 kOe with $\boldsymbol{H}$ along the y-axis, thus V cannot be attributed to magnetic-field-induced suppression of superconductivity.

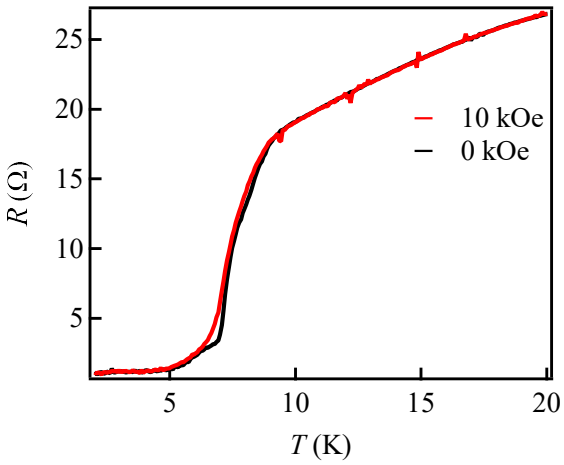

Fig. 2-2-5-5 Temperature dependence of the resistance, obtaining at 0 kOe and 10 kOe along the y-axis. The agreement of the two datasets demonstrated that the superconductivity of the κ-NCS device was almost unaffected up to10 kOe.

In order to investigate the spin diffusion length and further support the macroscopic pair of antiparallel spins, the author set nonlocal measurements, where the spin excitation area and the spin detection area were spatially separated at $\theta = 0$ (Fig. 2-2-5-6). This confirmed the diffusion of generated spin pairs and quantitative amount of the spin accumulation inside of κ-NCS more directly.

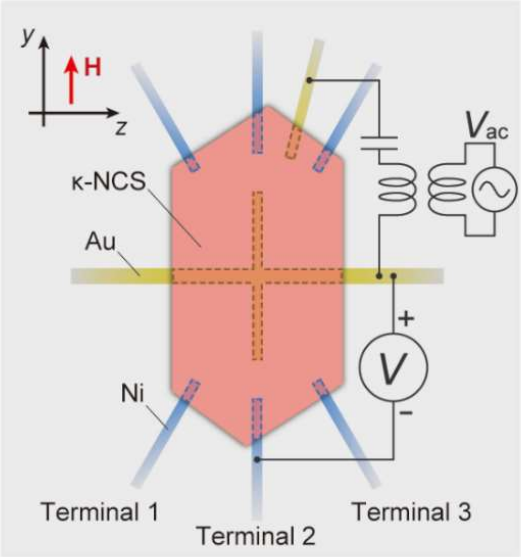

Fig. 2-2-5-6 Schematic illustration of the nonlocal measurement.

2-2-6 CD & Electrical Measurements in Device #2

The electrical measurement was performed with the standard four-probe method from 300 K to 2 K with an electric current of 10 μA and annealing was employed at 80 K for 1 day. And T_c was 7.5 K, which was the same temperature in device #1 (Fig. 2-2-6-1).

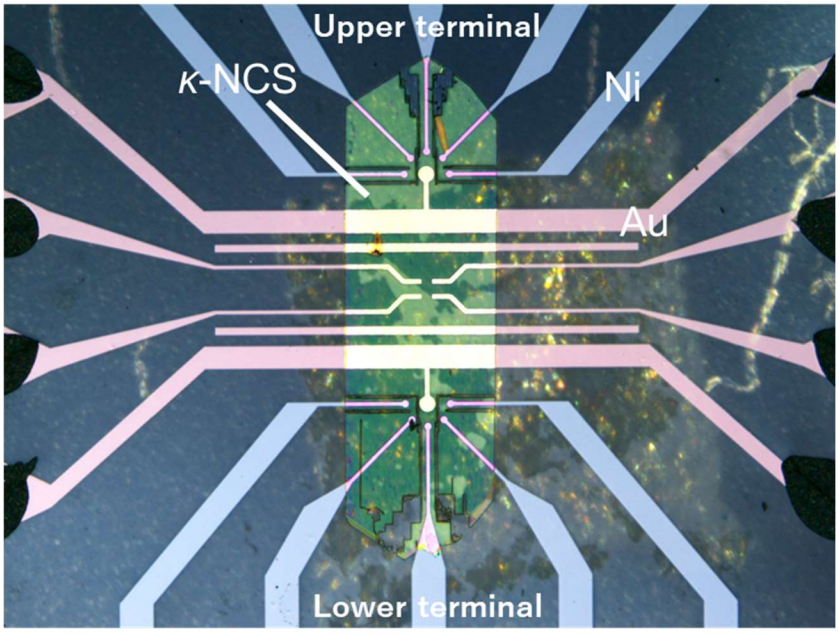

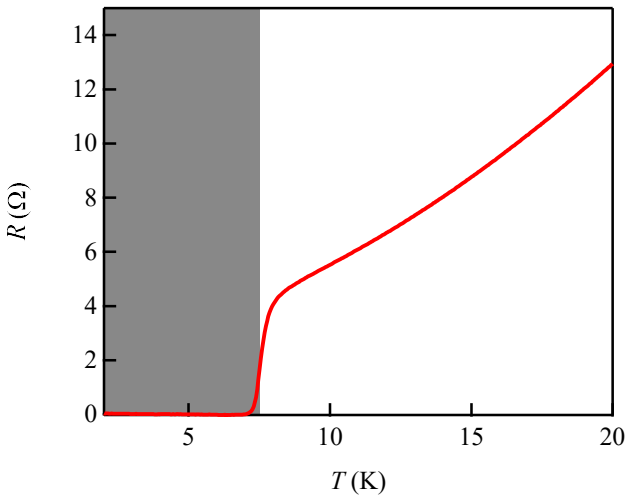

Fig. 2-2-6-1 Temperature dependence of resistance in device #2, where T_c = 7.5 K.

Nonlocal measurement was performed with device #2. Crystal has two domains with opposite handedness. In this measurement, $\boldsymbol{H}$ rotation (-60° < θ < 60°) from the y-axis within the crystal plane.

I_{ac} was applied to the two Au electrodes for excitation by AC power supply of setting to 1 $V_{p\text{-}p}$, 11.5 MHz.

2-3 Results and Discussion

2-3-1 Giant Spin Polarization

The authors have estimated the voltage value in a gyrotropic superconductor by Edelstein effect. The used material parameters of κ-NCS were the density of state at the Fermi level (50 eV^{-1} nm^{-3}); the superconducting transition temperature (7.5 K); the superconducting coherence length (7 nm); the critical electric current density (1000 A／cm^2); the magnitude of SOI (~ 1 nm^{-1}).

The point of group of κ-NCS is C_2. The corresponding $\boldsymbol{T}$ is given by

$$\boldsymbol{T} = \begin{pmatrix} T_{xx} & 0 & T_{xz} \\ 0 & T_{yy} & 0 \\ T_{zx} & 0 & T_{zz} \end{pmatrix}.$$

Since $\tilde{\boldsymbol{J}}_{\boldsymbol{e}}$ was applied along the y-axis, the only component of δn was $\delta n_y = T_{yy}\tilde{J}_e^y$ in this experiment. From the equation (3), T_{yy} ~ 10^{-4} nm^{-3} was obtained. Provided that cross-sectional area of the crystal was 100 μm^2, the supercurrent density was 10 A／cm^2. By normalizing the superconducting current density by the critical current density, $\tilde{J}_e^y$ ~ 10^{-2} was obtained. From the equation (1), δn_y was estimated to be at most 10^{-6} nm^{-3}. From the equation (2), V_{Edel} < 26 nV was calculated.

The used parameters as follows: Δ_0 = 0.0011375 eV K^{-1}, g_{p_F} = (0, 1 × cos φ, 1 × sin φ) meV, $\zeta(3)$ = 1.20205, $N(E_F)$ = 5.0 eV nm^{-3}, k_B = 8.617333262145 × 10-5 eV K^{-1}, T_c = 7.5 K.

From this calculation, the voltage drop with Ni electrodes expected only from Edelstein effect V_{Edel} is estimated as $V_{Edel} \sim P^F \delta n_{int}^F / \{eN_{min}^F(E_F)\}$ —— (4), where P^F denotes the equilibrium spin polarization, and $N_{min}^F(E_F)$ denotes the density of states for the minority spin at the Fermi level of nickel[13]. Here, P^F = 0.4, $N_{min}^F(E_F)$ = 22.85 eV^{-1} nm^{-3} denotes equilibrium spin polarization and density of state for minority spin at the Fermi level of Ni, respectively.

Crucially, V_{odd} was three orders of magnitude larger than estimated V_{Edel} ≈ 26 nV. This large voltage requires additional explanations other than the Edelstein effect, which may include an enhancement of spin orbit interactions (SOI). As one of the candidate explanations, one may think that electron-lattice interaction enhances conventional SOI

in superconducting CISS effect. The spin polarization density was three orders of magnitude larger than 10^{-6} nm^{-3} estimated from the Edelstein effect thus the spin polarization density was 10^{-3} nm^{-3}. The carrier density of κ-NCS was 1 nm^{-3} from the composition and the unit cell volume. Therefore, the spin polarization ratio was calculated as 0.1%.

2-3-2 Spin Orientation

V_{odd} from nickel to κ-NCS varies with θ, and it disappeared when $\boldsymbol{H}$ was perpendicular to $\boldsymbol{\sigma}$. V_{odd} reversed sign at a certain angle (θ_{V0}) as the magnetic field rotated. On one of the electrodes (Terminal 2 in Fig. 6), V_{odd} vanished at θ_{V0} = 17° and decreased from this angle with positive magnetic field rotation (Fig. 2-3-2-1). $\boldsymbol{\sigma}$ lay transversally at this angle. The two candidates can be found. One is 107° (17° + 90°). The other is -73° (17° - 90°). Considering the fact that the decrease in V_{odd} means $\boldsymbol{H}$ and $\boldsymbol{\sigma}$ directions are parallel, $\boldsymbol{H}$ must get close to be parallel to $\boldsymbol{\sigma}$ with positive magnetic field rotation in this electrode. 107° is calculated as $\boldsymbol{\sigma}$ with positive magnetic field rotation from θ_{V0} = 17°. The same analysis is applied to all the lower side electrodes: in Terminal 1, V_{odd} vanished at θ_{V0} = 12° thus $\boldsymbol{\sigma}$ was 102°. In Terminal 3, V_{odd} vanished at θ_{V0} = 29° thus $\boldsymbol{\sigma}$ was 119°. On another electrode (Terminal 5 in Fig. 6), V_{odd} vanished at θ_{V0} = 25° and increased from this angle with positive magnetic field rotation. Of the two candidates of $\boldsymbol{\sigma}$, one is 115° (25° + 90°) and the other is -65° (25° - 90°). $\boldsymbol{H}$ must get close to be antiparallel to $\boldsymbol{\sigma}$ with positive magnetic field rotation in the upper side electrodes. -65° is calculated as $\boldsymbol{\sigma}$ with positive magnetic field rotation from θ_{V0} = 25°. The same analysis is applied to all the upper side electrodes: in Terminal 4, V_{odd} vanished at θ_{V0} = 15° thus $\boldsymbol{\sigma}$ was -75°. In Terminal 6, V_{odd} vanished at θ_{V0} = 13° thus $\boldsymbol{\sigma}$ was -77° (Fig. 2-3-2-2). The pair of antiparallel spins at the two ends of the crystal were formed and the spin pairs were mutually oriented towards the outside of the crystal (Fig. 2-3-2-3). According to the theory of C_2 gyrotropic superconducting Edelstein effect, only 0° / 180° spin polarity must have been produced and these tilted spin polarities could not be explained. One possibility is inhomogeneously spread superconducting regions. The actual current application was not linear because the current passed through discretely scattered and connected superconducting regions. The other possibility is that CISS effect might be affected by g-factor of a BEDT-TTF molecule. In κ-NCS crystal structure, BEDT-TTF molecules are tilted by a dozen degrees from the conducting plane. As part of the spin theory, it might also be possible to involve a molecular g-factor.

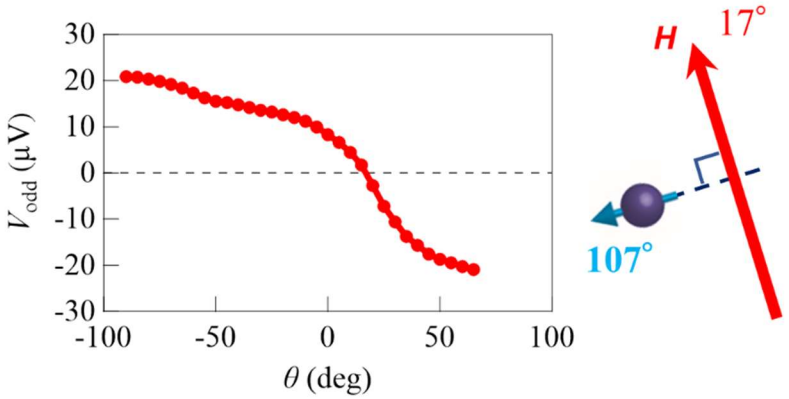

Fig. 2-3-2-1 Angular dependence of V_{odd}. The disappearance of the voltage at a magnetic field angle of 17° means that the spin is then lying perpendicular to it.

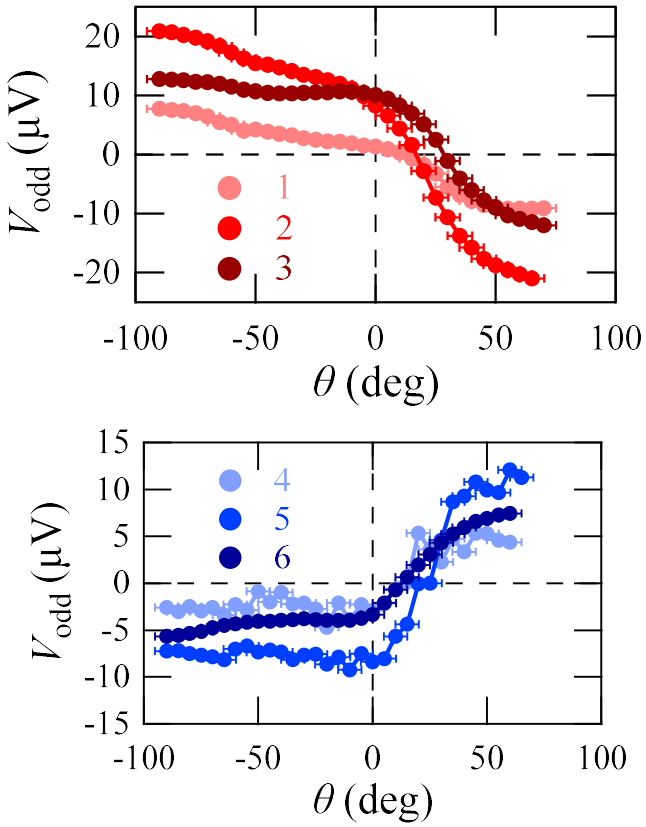

Fig. 2-3-2-2 Angular dependence of V_{odd} measured at the detection terminals.

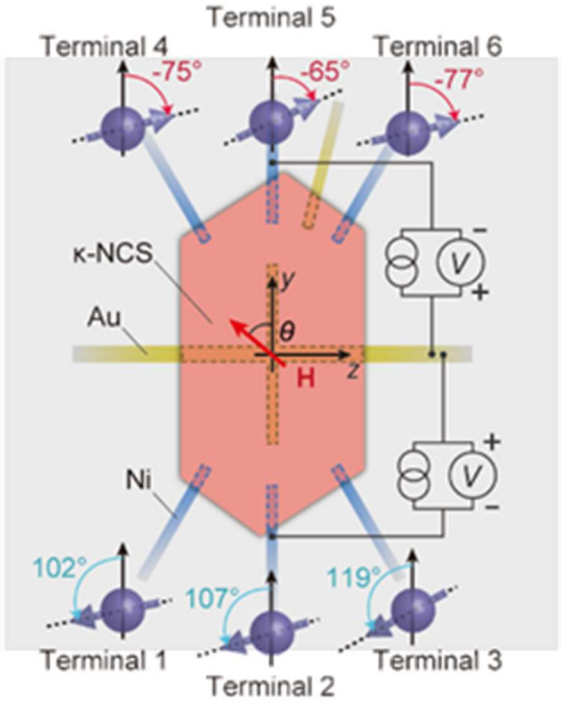

Fig. 2-3-2-3 Spatial distribution of the spin accumulation, showing a pair of antiparallel spins in whole of κ-NCS.

2-3-3 Spin Diffusion

Au electric current of 2.4 μA was applied between the two Au electrodes for excitation in the upper side of the crystal. V_{odd} was measured between the Au electrode and the Ni electrodes for detection in the lower side of the crystal. These excitation electrodes and detection electrodes were spatially separated by 600 μm. The input electric current was generated by AC power supply of setting to 100 $mV_{p\text{-}p}$. A nonlocal voltage signal appeared and exhibited the same magnetic field dependence as observed in the local measurement. Each V_{odd} of three terminals (Terminal 1, 2, 3) in this measurement was less than that in the local measurement. In Terminal 1, $V_{odd} \approx 0.4$ μV. In Terminal 2, $V_{odd} \approx 1$ μV. In Terminal 3, $V_{odd} \approx 0.5$ μV (Fig. 2-3-3-1). The offset voltage at zero field at each terminal has been removed (~ 0.2 μV).

The nonlocal measurements implied that the spins propagate to at least 600 μm without relaxation and spin polarization certainly prevails in a whole crystal.

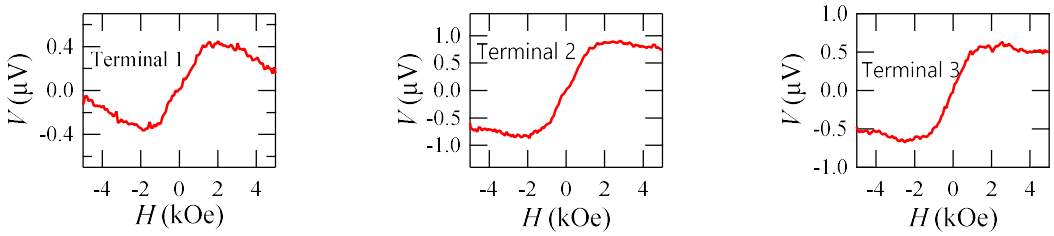

Fig. 2-3-3-1 Magnetic field dependence in the nonlocal measurements at the detection terminals. The voltage signals appeared even at the spin-detection terminals away from the spin-excitation terminals.

2-3-4 Spin Polarization Switching

In device #2, the crystal has two domains with opposite handedness. From the CD measurements, Area A was revealed as the blue region and Area B, C were revealed as the red regions.

I_{ac} was applied to Area A by AC power supply of setting to 1 $V_{p\text{-}p}$, 11.5 MHz. While nonlinear voltage signal was observed, the voltage did not reverse sign distinctly upon the reversal magnetic field. This seemed that a linear component was added to the voltage signal that came from the spin accumulation. One possibility of the linear component was EMChA. By linear fitting of the EMChA and subtracting its linear component manually at each angle, the spin-derived antisymmetric signal was obtained. Each $\boldsymbol{\sigma}$ was determined at the two ends of the crystal, considering sign change of $V_{odd} = [V(+1\,\mathrm{kOe}) - V(-1\,\mathrm{kOe})]/2$. Since V_{odd} was decreased from θ_{V0}, $\boldsymbol{H}$ and $\boldsymbol{\sigma}$ directions get to be parallel. In Upper terminal, V_{odd} vanished at θ_{V0} = -45° thus $\boldsymbol{\sigma}$ was -135°. In Lower terminal, V_{odd} vanished at θ_{V0} = -65° thus $\boldsymbol{\sigma}$ was 25°. The pair of antiparallel spins at the two ends of the crystal were formed and the spin pairs were mutually oriented outwards in the crystal.

I_{ac} was applied to Area B (blue CD region) by AC power supply of setting to 1 $V_{p\text{-}p}$, 11.5 MHz. As with the analysis of Area A, the spin-derived antisymmetric signal was obtained by linear fitting of the EMChA and subtracting its linear component. Each $\boldsymbol{\sigma}$ was determined at the two ends of the crystal, considering sign change of $V_{odd} = [V(+5\,\mathrm{kOe}) - V(-5\,\mathrm{kOe})]/2$. Since V_{odd} was increased from θ_{V0}, $\boldsymbol{H}$ and $\boldsymbol{\sigma}$ directions get to be antiparallel. In Upper terminal, V_{odd} vanished at θ_{V0} = 10° thus $\boldsymbol{\sigma}$ was 100°. In Lower terminal, V_{odd} vanished at θ_{V0} = 20° thus $\boldsymbol{\sigma}$ was -70°. The opposite spins at the two ends of the crystal were formed and the spin pairs were mutually oriented inwards in the crystal, which was opposite from the case of Area A (Fig. 2-3-4-1).

The orientation of the spin pair was inverted depending on the handedness of the excitation region and resulting in inward/outward spin paring switching. This handedness-dependent polarity conversion is evidence for spin accumulation generated by the CISS effect.

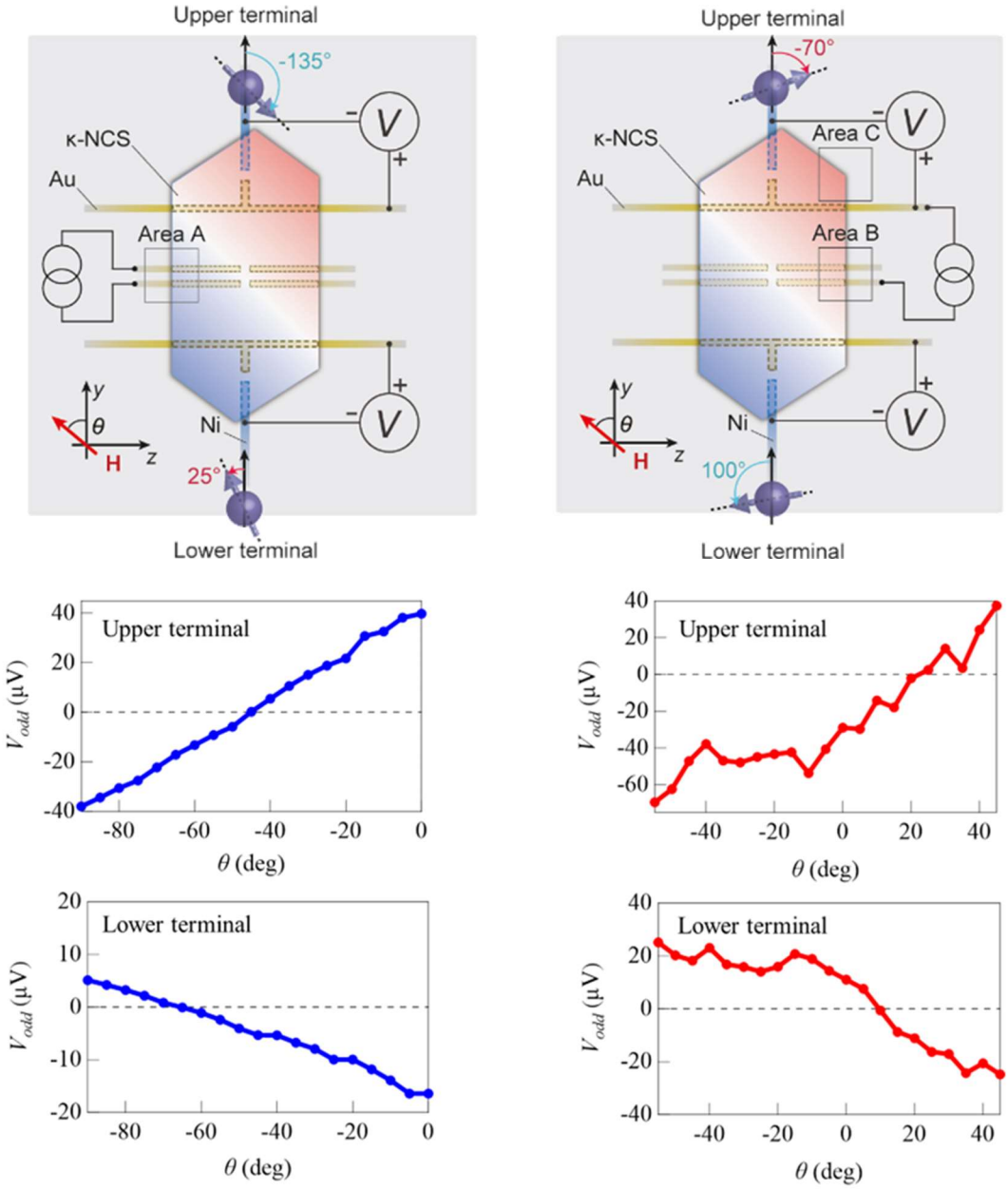

Fig. 2-3-4-1 Schematic of the experimental geometry for selective application of a.c. electric currents through one of the two domains and angular dependence of V_{odd} in the nonlocal measurements. The angles of the spin polarization were determined, considering sign change of the voltage.

2-3-5 Interface Transparency

Supposing that rectification occurs in the circuit, V would be unintentionally observed at the capacitor in this arrangement. Between Terminal 2 and the Au electrode of sample #1, a d.c. electric current was applied for the range of ± 2 μA at 7.5 K (Fig. 2-3-5-1). A linear current-voltage curve was clearly obtained (Fig. 2-3-5-2). The fact V was the odd function with respect to I means that rectification did not occur in this circuit. This result precludes the possibilities that the voltage signals simply originate from a rectification between the Ni and Au contacts with κ-NCS.

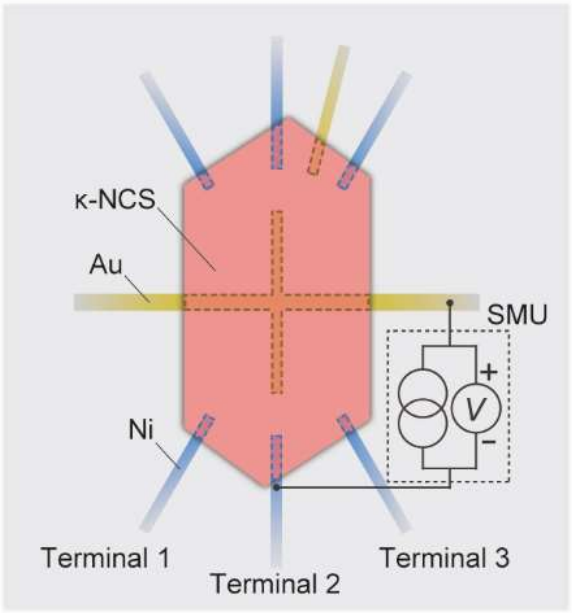

Fig. 2-3-5-1 Schematic of the experimental geometry in d.c. measurements. SMU denotes a source measure unit.

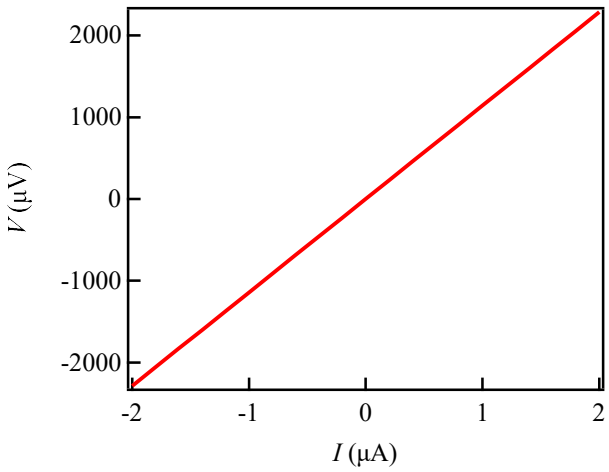

Fig. 2-3-5-2 Voltage-current curve that obtained by d.c. measurements. The agreement of the dataset demonstrated the absence of charge rectification at the interface between the Au-capped Ni electrode and κ-NCS.

2-3-6 Possible Spin Carrier

The temperature (T) dependence of V_{odd} around a superconducting transition temperature was performed. V_{odd} appeared in the vicinity of T_c and was largest at the middle of the transition. V_{odd} did not appear in the metallic state in the high temperature region. This indicates that macroscopic coherence length is necessary to generate spin via CISS effect. In the lower temperature region than T_c, V_{odd} disappeared as well (Fig. 2-3-6-1). One possibility is caused by a conductance mismatch problem. Spin transport between two materials with different conductivities can be disturbed. Ni has much lower conductivity than κ-NCS. Spins cannot be detected at the electrode. The other possibility is that the origin of spin carrier is Bogoliubov quasiparticle, which forms with Cooper pair formation at the transition temperature. In lower temperatures, the Bogoliubov quasiparticles become fully Cooper pairs and no spins are observed. However, the origin of spin carrier is unidentified.

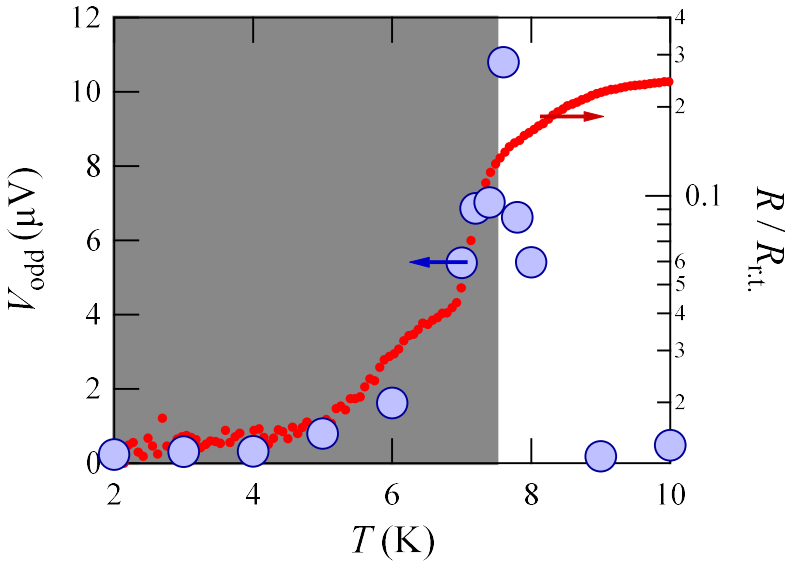

Fig. 2-3-6-1 Temperature dependence of the voltage signal around the superconducting transition temperature.

2-3-7 Frequency dependence

Resonance in circuits means that a voltage or current exhibits extreme values at a certain frequency. The impedance equation is given as follow: $Z = \sqrt{R^2 + \left(\omega L - \frac{1}{\omega C}\right)^2}$, where R denotes resistance, ω denotes angular velocity, L denotes inductance, and C denotes capacitance. At a specific $\omega = 2f\pi$, an inductance of a coil and a reactance of a capacitor cancel each other out and the impedance becomes minimum, where largest current I_{ac} can be produced.

The frequency (f) dependence of V under $\boldsymbol{H}$ along the y-axis was performed. I_{ac} was applied to Area A by AC power supply of setting to 1 V. The frequency was modulated from 1 MHz to 30 MHz by 500 kHz, and V was measured by changing $\boldsymbol{H}$ by ± 5 kOe at each frequency. In both of Upper and Lower terminal, the largest V_{odd} was obtained at 11.5 MHz (Fig. 2-3-7-1). This signal enhancement may originate in the above resonance circuit of the measurement system.

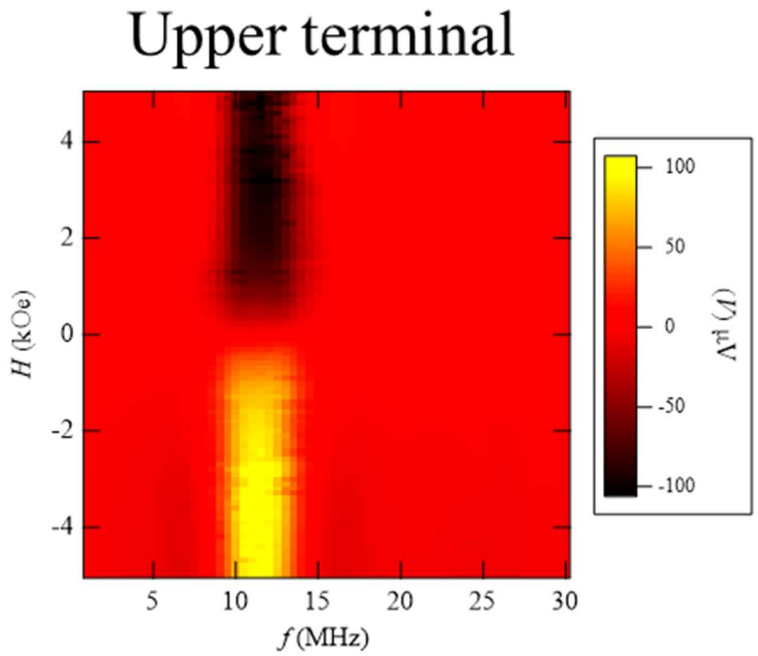

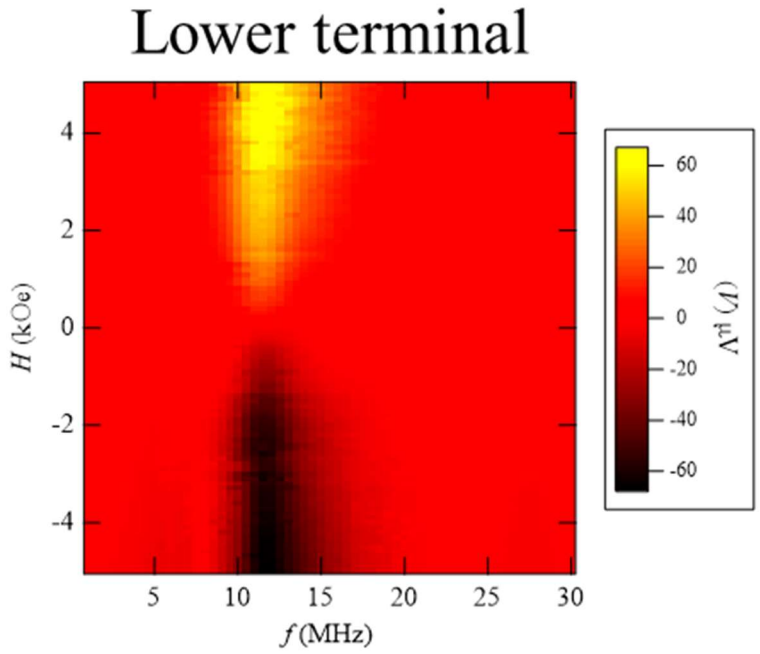

Fig. 2-3-7-1 Frequency dependence of the voltage signal intervals of 500 kHz. The largest V_{odd} was obtained at 11.5 MHz in this device setup.

2-3-8 Symmetry Consideration

The inward/outward switching of a pair of antiparallel polarized spins can be performed both by the time-reversal (T) operation and by the mirror (m) operation, which is regarded as T-odd chirality. On the other hand, a typical concept of CISS effect, which is a spin polarization of electron tunneling through a chiral molecule, accompanies only T-even quantities because the helicity of electron produced by CISS effect does not change its sign under T (opposite direction current through a chiral molecule produces a spin current with the opposite direction) (Fig. 2-3-8-1). It seems this is also the case in the first step of the present experiment with a chiral superconductor.

In order to understand these two facts in a consistent way, a transformation of T-even spin current into a T-odd antiparallel spin pair needs to be involved in the second step of the present system. In other words, the results proved that spin can reflect lattice chirality in a chiral superconductor through CISS effect and T-even chirality to T-odd chirality conversion was shown to be feasible. This would confirm the antiparallel spin pair hypothesis proposed for the molecular CISS effect, with which enantio-separation is also possible at the surface of magnet, through a superconductor with chiral lattice in a macro-scale experiment.

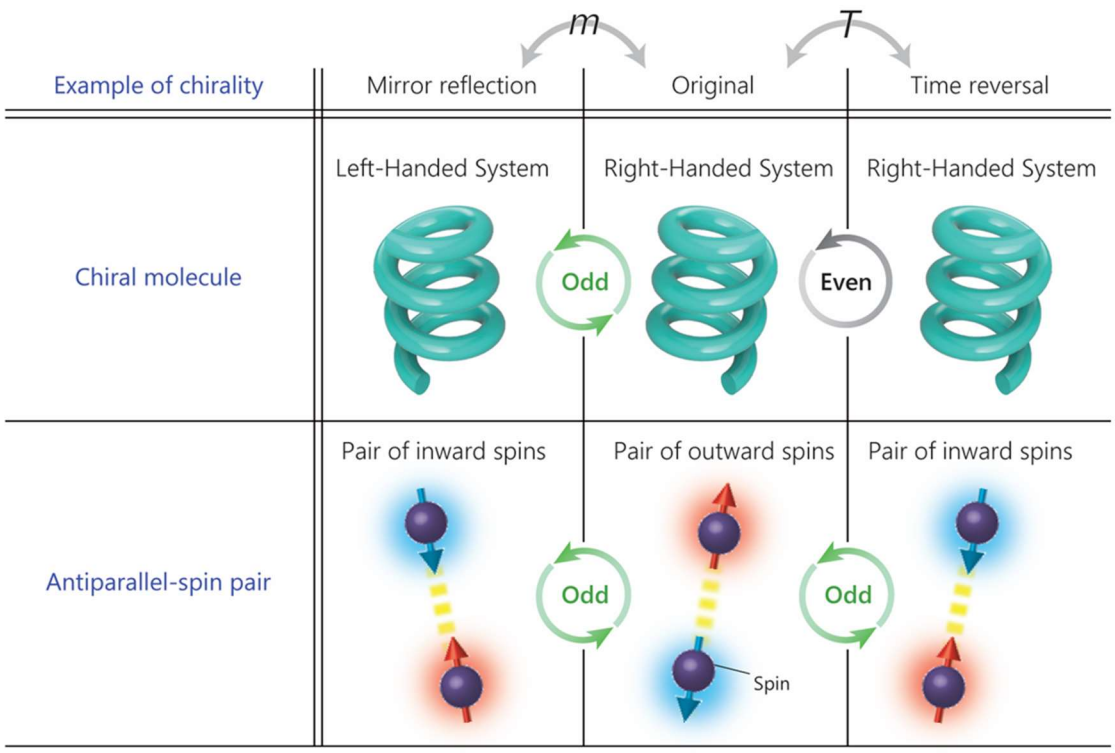

Fig. 2-3-8-1 Transformation of a chiral molecule and a pair of antiparallel spins under mirror reflection (m) and time-reversal(T).

§4 Concluding Remarks

This dissertation considers the possibilities of generating spin-polarized supercurrent, its high polarization rate, and polarity reversal by switching the chirality.

The primary problem is the intrinsic nature of a superconductor where Cooper pair is singlet. Chiral molecular materials can emit a spin-polarized current with a high polarization rate despite its constituent light elements. This effect is known as a chiral-induced spin selectivity (CISS) effect. However, no theoretical consensus has been achieved.

A pair of antiparallel spins cannot be superimposed onto its mirror image thus exhibits chirality, corresponding to a chiral molecule. In order to investigate a pair of antiparallel spins that may elucidate the origin of CISS effect, a chiral superconductor where macroscopic coherence is given by superconductor is suitable for measurements.

The author has prepared thin crystals of a chiral molecular superconductor κ-NCS. This material had non-centrosymmetric space group $P2_1$. The author prepared device #1, where the crystal carries a spatially uniform enantiomorphic excess. By applying a.c. electric currents to device #1, a spin-dependent voltage drop was observed. Superconductors with macroscopic coherence lengths beyond the unit cell enabled electron spin to feel the chirality derived from the molecular lattice. From this observation, the CISS effect in the chiral superconductor was confirmed.

In a gyrotropic superconductor, it is theoretically predicted that spin-polarized current is generated in a specific direction by a group of points upon application of an electric current. Nevertheless, κ-NCS produced the spin-polarized current of which polarization rate was three orders of magnitude larger than the conventional theory in the author's measurement. To rationalize this large value, one might think that CISS effect includes a mechanism to enhance the spin-orbit interaction.

The author investigated the spin orientation by measuring the in-plane angular dependence of the interface voltage. The pair of antiparallel spins at the two ends of the crystal were confirmed. Macroscopic size of the superconducting state with electron coherence enabled spatial mapping of spin accumulation. The fact that κ-NCS not only produced spin-polarized currents but also caused spin accumulation implies that T-odd spin-based chirality can be generated in a spin reservoir of the superconductor. This would suggest that CISS effect in molecules also involves conversion from T-even to T-odd chirality.

Furthermore, A spin-dependent voltage drop was confirmed even when the spin excitation area and the spin detection area were spatially separated by 600 μm. This nonlocal measurement suggests that the spins diffuse over several hundred micro meters without relaxation and spin polarization certainly prevails in a whole crystal.

In addition, the author prepared device #2, where domains of opposite handedness coexist. When spins were produced at different chiral domains, a pair of antiparallel spins in opposite directions were observed. Thus, inward/outward spin pairing switching was achieved by switching handedness of κ-NCS at the excitation positions.

As a consequence, it was figured out that a chiral superconductor has an ability to generate giant spin polarization. Hence the present research has provided clear methods for generation and switching of spin current in the superconducting state and can be extended to superconducting spintronics. At the same time, an experimental link between time-reversal symmetry and chirality in CISS effect has been suggested. It was shown that T-even chirality to T-odd chirality conversion may be feasible.

References

[1] J. Linder, *et al*., *Nature Phys.*, **11**, 307 (2015).

[2] K. Ray, *et al*., *Science*, **283**, 814 (1999).

[3] M. N. Baibich, *et al.*, *Phys. Rev. Lett.*, **61**, 2472 (1988).

[4] (1) M. I. Dyakonov and V. I. Perel, *Phys. Lett. A*, **35**, 459 (1971). (2) Y. Kato, *et al.*, *Science*, **306**, 1910 (2004). (3) J. E. Hirsch, *Phys. Rev. Lett.*, **83**, 1834 (1999).

[5] K. Uchida, *et al.*, *Nature*, **455**, 778 (2008).

[6] (1) N. S. Averkiev and M. I. Dyakonov, *Sov. Phys. JETP Lett.*, **35**, 196 (1983). (2) A. A. Bakun, *et al.*, *Sov. Phys. JETP Lett.*, **40**, 1293 (1984).

[7] J. Flipse, *et al.*, *Phys. Rev. Lett.*, **113**, 027601 (2014).

[8] Yu. A. Bychkov and E. I. Rashba, *Sov. Phys. JETP Lett.*, **39**, 78 (1984).

[9] V. M. Edelstein, *Solid State Commun.*, **73**, 233 (1990).

[10] K. Izawa, *et al.*, *Phys. Rev. Lett.*, **88**, 027002 (2001).

[11] V. M. Edelstein, *Phys. Rev. Lett.*, **75**, 2004 (1995).

[12] W. -Y. He, *et al.*, *Phys. Rev. Res.*, **2**, 012073(R) (2020).

[13] S. Maekawa, *et al.*, *Spin Current* (Oxford Univ. Press, 2015).

[14] R. Naaman and D. H. Waldeck, *J. Phys. Chem. Lett.*, **3**, 2178 (2012).

[15] (1) B Göhler, *et al.*, *Science*, **331**, 894 (2011). (2) P. V. Möllers, et al., Isr. J. Chem., **62**, e2022000 (2022).

[16] G. L. J. A. Rikken, et al., *Phys. Rev. Lett.*, **87**, 236602 (2001).

[17] F. Qin, et al., *Nat. Commun.*, **8**, 14465 (2017).

[18] D. Dew-Hughes, *Rep. Prog. Phys.*, **34**, 821 (1971).

[19] (1) H. Urayama, *et al.*, *Chem. Lett.*, **17**, 55 (1988). (2) K. Nozawa, *et al.*, *Chem. Lett.*, **17**, 617 (1988).

[20] N. N. Bogoljubov, *Il Nuovo Cimento*, **7**, 794 (1958).

[21] J. Ferraris, *et al.*, *J. Am. Chem. Soc.*, **95**, 948 (1973).

[22] (1) M. Mizuno, *et al.*, *J. Chem. Soc., Chem. Commun.*, 18 (1978). (2) S. S. P. Parkin, *et al.*, *Phys. Rev. Lett.*, **50**, 270 (1983). (3) E. B. Yagubskii, *et al.*, *JETP Lett.*, **39**, 12 (1984).

[23] S. Fujio, *et al.*, *J. Appl. Crystallogr.*, **42**, 433 (2009).

[24] N. F. Mott and R. Peierls, *Proc. Phys. Soc.*, **49**, 72 (1937).

[25] J. M. Bijvoet, *et al.*, *Nature*, **168**, 271 (1951).
[26] T. Narushima and H. Okamoto, *Sci. Rep.*, **6**, 35731 (2016).

Publication

R. Nakajima, *et al.*, Giant spin polarization and a pair of antiparallel spins in a chiral superconductor, *Nature*, **613**, 479 (2023).

ACKOWLEDGEMENTS

I express my sincere thanks to Prof. Hiroshi M. Yamamoto for supporting my research and giving me an enormous amount of knowledge with a warm heart and generous spirit. Undoubtedly, it is a turning point in my life. I am honored to join Yamamoto group in The Institute for Molecular Science.

And I am also grateful to Assis. Prof. Daichi Hirobe and Assis. Prof. Takuro Sato for providing me with the measurement and analysis programs and giving me lots of knowledge. I have gained a better understanding of the fundamentals of physics.

In addition, I would like to thank Mr. Yoji Nabei for collecting the data on CD imaging.

And I am grateful to Prof. Hiromi Okamoto and Assis. Prof. Tetsuya Narushima for cooperating with CD measurements.

Also, I am grateful to the Equipment Development Center and the Instrument Center (The Institute for Molecular Science) for technical support.

Finally, I would like to thank my family: my father, my mother, my aunts, my uncle, my grandparents, and everyone involved with me.

January 26th, 2023

Ryota Nakajima